

"THE  ${}^4\text{He}(\vec{d},p){}^4\text{He}$  REACTION, SINGLE-PHOTON  
EMISSION FOLLOWING PROTON-INDUCED DOUBLE  
K-SHELL IONIZATION AND A DESIGN AND  
FEASIBILITY STUDY FOR A PROTON MICROPROBE".

BY

MUTHANA SABBAR ABDUL LATIF AL-GHAZI

A THESIS

Submitted to the Faculty of Graduate Studies  
in Partial Fulfilment of the Requirements  
for the Degree of

DOCTOR OF PHILOSOPHY

Department of Physics

University of Manitoba

Winnipeg, Manitoba

January 1983

THE  ${}^4\text{He}(\vec{d},p){}^4\text{He}$  REACTION, SINGLE-PHOTON  
EMISSION FOLLOWING PROTON-INDUCED DOUBLE  
K-SHELL IONIZATION AND A DESIGN AND  
FEASIBILITY STUDY FOR A PROTON MICROPROBE

BY

MUTHANA SABBAR ABDUL LATIF AL-GHAZI

A thesis submitted to the Faculty of Graduate Studies of  
the University of Manitoba in partial fulfillment of the requirements  
of the degree of

DOCTOR OF PHILOSOPHY

© 1983

Permission has been granted to the LIBRARY OF THE UNIVER-  
SITY OF MANITOBA to lend or sell copies of this thesis, to  
the NATIONAL LIBRARY OF CANADA to microfilm this  
thesis and to lend or sell copies of the film, and UNIVERSITY  
MICROFILMS to publish an abstract of this thesis.

The author reserves other publication rights, and neither the  
thesis nor extensive extracts from it may be printed or other-  
wise reproduced without the author's written permission.



"...But I will leave the reader unmoved  
and proceed with the object before me. That  
object is to give a plain account of my  
...findings..."

(Charles Dickens: The Holly-Tree)

ABSTRACT

Three separate projects are described in this thesis. The first chapter deals with measurements of deuteron vector and tensor analysing powers ( $A_y$  and  $A_{yy}$ ) in the  ${}^4\text{He}(\vec{d},p){}^4\text{He}$  reaction. The purpose of this work was mainly to provide deuteron tensor analysing powers for this reaction. The vector analysing powers were necessary for comparison with existing data and theoretical calculations. The work is prompted by a recent formulation of the deuteron-alpha system as a three-body problem. This theory was successful in describing the elastic scattering process. More interesting, however, is the case of deuteron breakup. Here the theory reproduces the proton double scattering cross-section ( $d^2\sigma_p/d\Omega_p dE_p$ ) in shape and magnitude quite well at 15 MeV. The theory however predicts the shape of the deuteron vector analysing powers ( $A_y$ ) but not the magnitude. This is especially true at proton back angles. More recently the angular distribution of the tensor analysing powers ( $T_{20}$ ,  $T_{21}$  and  $T_{22}$ ) in the vicinity of the final state interaction (FSI) peak corresponding to the  ${}^5\text{He}_{g.s.}$  showed disagreement with theory. Therefore it was decided to direct the present investigation towards the study of as wide a range of the proton distribution as possible. It is found that the disagreement between theory and experiment persists over the entire range of proton energies and scattering angles investigated. The source of the disagreement is attributed to the fact that the theory lacks the basic ingredients necessary for the description of tensor polarisation observables in this reaction. Some suggestions of further calculations and experimental measurements necessary to resolve the discrepancy are made.

In chapter two the subject of single-photon emission following proton-induced double K-shell ionization is addressed. The theoretical description of the process is critically examined and the assumptions involved in the formulation of the phenomenon are discussed. Some numerical calculations based on existing models are carried out. The results obtained are subjected to an experimental test in a suitably designed experiment. It is concluded that the existing theory overestimates the probability of occurrence of the process. The experimental result obtained for rubidium sheds some light on the validity of approximation methods suggested in the literature to predict the double ionization probability. The material covered in this chapter has appeared in the literature recently (Al-Ghazi et al., 1982).

The final chapter is a design project. It deals with the design and feasibility study of a device which may be thought of as a "proton microscope". This device is commonly called a proton microprobe. As a prelude to the design study, the usefulness of K x-rays induced by 20-50 MeV protons as an analytical tool in the study of medium and heavy elements is discussed. A case is presented for the establishment of a proton microprobe at the University of Manitoba Cyclotron Laboratory. The design features of such a facility and its specifications are outlined. The immediate applications of the instrument and its relevance to research programs at the University of Manitoba are summarised. This project has been the subject of two publications (Al-Ghazi and McKee, 1982 and Al-Ghazi et al., 1979).

### ACKNOWLEDGEMENTS

The author wishes to express his gratitude to Dr. J.S.C. McKee for extending the facilities of the Cyclotron Laboratory of the University of Manitoba where this research was carried out and for Dr. McKee's keen interest in the projects described in this thesis, his effective supervision, guidance and unfailing support throughout the course of these investigations.

It is a pleasure to thank Dr. J. Birchall who has contributed a great deal of advice and practical help without which these projects would not have been brought to a conclusion.

Members of the so-called (PIXE-neutron) research group (past and present), particularly Claude Lapointe and Nelson Videla, have been understanding and supportive. They contributed a considerable amount of their time during the painstaking stage of data taking. Their splendid efforts must not go unacknowledged.

The help and advice of the Computer Services Division of the Cyclotron Laboratory, particularly the efforts of Mr. J.R. Anderson and Dr. C.A. Smith are greatly appreciated. Dr. Smith kindly provided the program "POLCA" which was used to analyse the data of chapter one of this thesis.

Thanks are also due to members of the Cyclotron Laboratory support staff and Mechanical and Electrical workshop personnel of the Department of Physics for their advice and help during various stages of the work.

The final phase of writing this document was carried out while the author was on the teaching staff of the Physics Department of the University of Toronto. The encouragement of colleagues and in particular Professors R.E. Azuma and A.W. Key is appreciated.

Margaret Currie has typed this thesis with cheerful expediency.

Financial support from the Natural Sciences and Engineering Research Council of Canada and the University of Manitoba made it possible for the author to undertake this program of study.

TABLE OF CONTENTS

|  | <u>PAGE</u> |
|--|-------------|
| QUOTATION  | i           |
| ABSTRACT   | ii          |
| ACKNOWLEDGEMENTS   | iv          |
| TABLE OF CONTENTS  | vi          |
| LIST OF FIGURES  | viii        |
| LIST OF TABLES   | x           |
| <u>CHAPTER ONE: THE <math>{}^4\text{He}(\vec{d},p)n{}^4\text{He}</math> REACTION</u> | 1           |
| 1.1 INTRODUCTION   | 2           |
| 1.2 THEORY   | 9           |
| 1.3 EXPERIMENT   | 13          |
| 1.3.1 The Deuteron Beam  | 13          |
| 1.3.2 Experimental Setup   | 16          |
| 1.3.3 Electronics  | 19          |
| 1.3.4 Procedure  | 22          |
| 1.3.5 Data Analysis  | 25          |
| 1.4 RESULTS AND DISCUSSION   | 37          |
| 1.5 FURTHER WORK   | 43          |
| <u>CHAPTER TWO: SINGLE-PHOTON EMISSION FOLLOWING</u>                                 |             |
| <u>PROTON-INDUCED DOUBLE K-SHELL</u>   |             |
| <u>IONIZATION OF RUBIDIUM</u>  | 45          |
| 2.1 INTRODUCTION   | 46          |
| 2.2 THEORY   | 50          |
| 2.2.1 Double K-Shell Vacancy Production  | 50          |
| 2.2.2 The Branching Ratio  | 52          |
| 2.2.3 Criteria for the Experiment  | 55          |

|  | <u>PAGE</u> |
|--|-------------|
| 2.3 EXPERIMENT   | 58          |
| 2.3.1 Apparatus  | 58          |
| 2.3.2 The Rubidium Target  | 59          |
| 2.3.3 The Absorber   | 59          |
| 2.3.4 The HPGe Detector  | 61          |
| 2.3.5 Electronics  | 63          |
| 2.4 EXPERIMENTAL PROCEDURE   | 66          |
| 2.4.1 Spectrum Calibration   | 66          |
| 2.4.2 Beam Monitoring  | 66          |
| 2.4.3 Single-Photon Search   | 67          |
| 2.4.4 Data Analysis  | 68          |
| 2.5 RESULTS AND CONCLUSIONS  | 75          |
| <br><u>CHAPTER THREE: DESIGN AND FEASIBILITY STUDY</u>   |             |
| <u>OF A PROTON MICROPROBE FOR K</u>  |             |
| <u>X-RAY STUDIES</u>   |             |
| 3.1 THE ROLE OF K X-RAYS AS AN ANALYTICAL TOOL   | 76          |
| 3.2 DESIGN CONSIDERATIONS  | 77          |
| 3.3 APPLICATIONS   | 80          |
| 3.4 CONCLUSIONS  | 91          |
| APPENDIX A: CORRECTION FOR THE VECTOR POLARISATION<br>IN THE "m=0" STATE   | 92          |
| APPENDIX B: DEUTERON VECTOR AND TENSOR ANALYSING<br>POWERS OF THE ${}^4\text{He}(\vec{d},p){}^4\text{He}$ REACTION<br>AT 14.8 MeV INCIDENT DEUTERON ENERGY | 94          |
| APPENDIX C: A POST-SUBMISSION NOTE IN CONNECTION<br>WITH CHAPTER ONE   | 96          |
| REFERENCES   | 101         |
|  | 102         |

LIST OF FIGURES

| <u>FIGURE</u> | <u>TITLE</u>   | <u>PAGE</u> |
|---------------|--|-------------|
| 1.1           | Feynman Diagrams representing quasi-free scattering, final state interaction and their interference.   | 5           |
| 1.2           | Cyclotron Beam Line Layout.  | 15          |
| 1.3           | Experimental Setup used in the ${}^4\text{He}(\vec{d},p)n{}^4\text{He}$ reaction studies.  | 18          |
| 1.4           | $\Delta E$ -E particle identification telescope and associated electronic circuit.   | 20          |
| 1.5           | Typical proton spectra obtained in ${}^4\text{He}(\vec{d},p)n{}^4\text{He}$ reaction studies.  | 23          |
| 1.6           | Deuteron vector analysing powers ( $A_y$ ) resulting from ${}^4\text{He}(\vec{d},p)n{}^4\text{He}$ reaction.   | 33          |
| 1.7           | Deuteron tensor analysing powers ( $A_{yy}$ ) resulting from ${}^4\text{He}(\vec{d},p)n{}^4\text{He}$ reaction.  | 35          |
| 2.1           | Ion-atom collision in the binary-encounter model.  | 51          |
| 2.2           | Energy level diagram showing decay of doubly ionized K-Shell by hypersatellite ( $K_{\alpha}^h$ ) and two-electron single-photon ( $K_{\alpha\alpha}^h$ ) transitions. | 54          |

|     | <u>PAGE</u>   |
|-----|---|
| 2.3 | Experimental setup used for two-electron<br>single-photon studies. 60                       |
| 2.4 | Electronics diagram of the circuit used in<br>the two-electron single-photon experiment. 65 |
| 2.5 | Single-photon energy spectrum. 69   |
| 3.1 | Focusing the proton beam from the cyclotron<br>to millimetre dimensions. 81                 |
| 3.2 | Layout of the proposed proton micropobe. 85   |
| 3.3 | Types of slit designs investigated for use<br>as collimators. 89                            |

LIST OF TABLES

| <u>TABLE</u> | <u>TITLE</u>   | <u>PAGE</u> |
|--------------|--|-------------|
| 1.1          | Geometrical parameters of the collimation system used in the ${}^4\text{He}(\vec{d},p)n{}^4\text{He}$ reaction experiment.   | 17          |
| 1.2          | Vector and tensor analysing powers of ${}^4\text{He}(\vec{d},d){}^4\text{He}$ reaction at 14.8 MeV and 15 MeV.   | 26          |
| 2.1          | Theoretical predictions of single-photon transition to normal $K_{\alpha}$ x-ray intensity ratio.  | 56          |
| 2.2          | Parameters relating to the choice of the absorber material.  | 62          |
| 2.3          | Single-photon results.   | 74          |
| 3.1          | Quadrupole field strength as a function of proton beam energy.   | 83          |
| 3.2          | Current on target as a function of collimator diameter.  | 86          |
| 3.3          | Beam parameters.   | 88          |
| A.1          | Measured values of $\delta^+$ at each angle.   | 95          |
| B.1-B.4      | Numerical values of deuteron vector and tensor analysing powers of the ${}^4\text{He}(\vec{d},p)n{}^4\text{He}$ reaction reported in figures (1.6) and (1.7) of the main text. | 97-100      |

CHAPTER ONE

THE  ${}^4\text{He}(\vec{d},p)n{}^4\text{He}$  REACTION

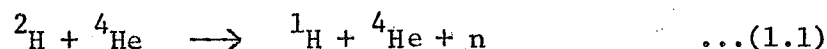
## 1.1 INTRODUCTION

The formulation of the three-body problem by Faddeev (1961) has made the problem tractable. The simplest of three-body systems is that of three non-relativistic identical spinless particles interacting pairwise through a two-body potential. This system has been successfully solved along the lines of the Faddeev treatment by Humberston et al., (1968), as a first step towards understanding the more fundamental problem of three nucleons interacting through the nuclear force. Much work has been devoted to this system in the past twenty years both experimentally and theoretically and progress made in the field has been the subject of many review articles. The clearest account of the three-body problem in nuclear physics known to this author is that of McKee (1970). Despite the advances made in the field of three-nucleon physics, the three-nucleon system remains a rather complex one to study. There are many factors which enter into its formulation; Pauli principle, spin structure in the initial and final states, Coulomb effects, etc. On the other extreme the three-boson system does not yield itself to experimental investigation.

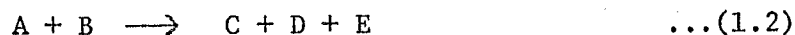
Recently, it has been pointed out that there are several advantages in studying the deuteron-alpha system as a three-body system (e.g. Nakamura et al., 1978, Dasgupta et al., 1980, Koike, 1980). In deuteron breakup reactions the final state is composed of a  $(n + \alpha + p)$ . The alpha particle may be considered as a structureless boson up to 30 MeV incident deuteron energy to a good approximation. Furthermore, the distinguishability of all three particles in the final state, the

relative simplicity of the spin structure (1+0) of the system and the fact that one of the particles (the neutron) is neutral are added attractions.

From the experimental point of view, the availability of polarised deuteron beams from polarised sources makes it possible to obtain a wealth of information on the (n +  $\alpha$  + p) system through the study of the reaction:



Having a polarised deuteron beam means one can measure polarisation observables, as well as cross sections, in a variety of kinematical conditions and experimental configurations, concentrating on various regions of phase space of the three body final state. The present chapter is a report on measurement of proton vector and tensor analysing powers ( $A_y$  and  $A_{yy}$ ) of the  ${}^4\text{He}(\vec{d}, p){}^4\text{He}$  reaction, carried out at the University of Manitoba Cyclotron Laboratory, using the polarised deuteron beam available from the Lamb-shift polarised ion source. The justification for the present study is presented later in this section. Before this task is undertaken attention is drawn to the fact that the reaction stated in equation (1.1) is of the type:



It is possible for two of the reaction products (e.g. C + D) to rescatter, or interact, in the final state, given the right conditions. Since this is of interest in the present investigation, as will be clear very shortly, a few general remarks on final state interactions are in order. For more details the reader is referred to the two

excellent reviews of Slobodrian (1971) and McKee (1973).

Figure (1.1) (taken from McKee, 1973 as is the discussion of this paragraph) is a diagrammatic representation of equation (1.2). If the centre of mass kinetic energy of the projectile is much larger than the binding energy of the target constituents, then the two body amplitude may be approximated by the free two body scattering amplitude. This is known as quasifree scattering (QFS) and is described by the impulse approximation (Figure 1.1.a). Final state interaction (FSI) results when two of the particles produced in the final state have very small or zero relative momentum (Figure 1.1.b). This is normally seen as an enhancement at the high momentum (or energy) edge of the phase space distribution of the third particle. Finally, it is possible for QFS to be modified by FSI and this is described in figure (1.1.c).

It is relevant to note at this point that the discrepancy reported by Nakamura et al. (1978) between experiment and the modified impulse approximation predictions for the  ${}^4\text{He}(\vec{d},p){}^4\text{He}$  at an incident deuteron energy of 15 MeV is, perhaps, to be expected since condition (a) of figure (1.1) is not fulfilled. The disagreement between theory and experiment is clearly seen in the cross-section at proton angles larger than  $40^\circ$ . The behaviour in the analysing power is less clear. At proton angles less than  $35^\circ$  the magnitudes of theoretical and experimental results are roughly equal but the shapes are not similar. For proton laboratory angles in the range of  $35^\circ$  to  $65^\circ$  theory and experiment agree very well, while only the shapes of the experimental analysing powers are reproduced by the theory. Indeed, it was

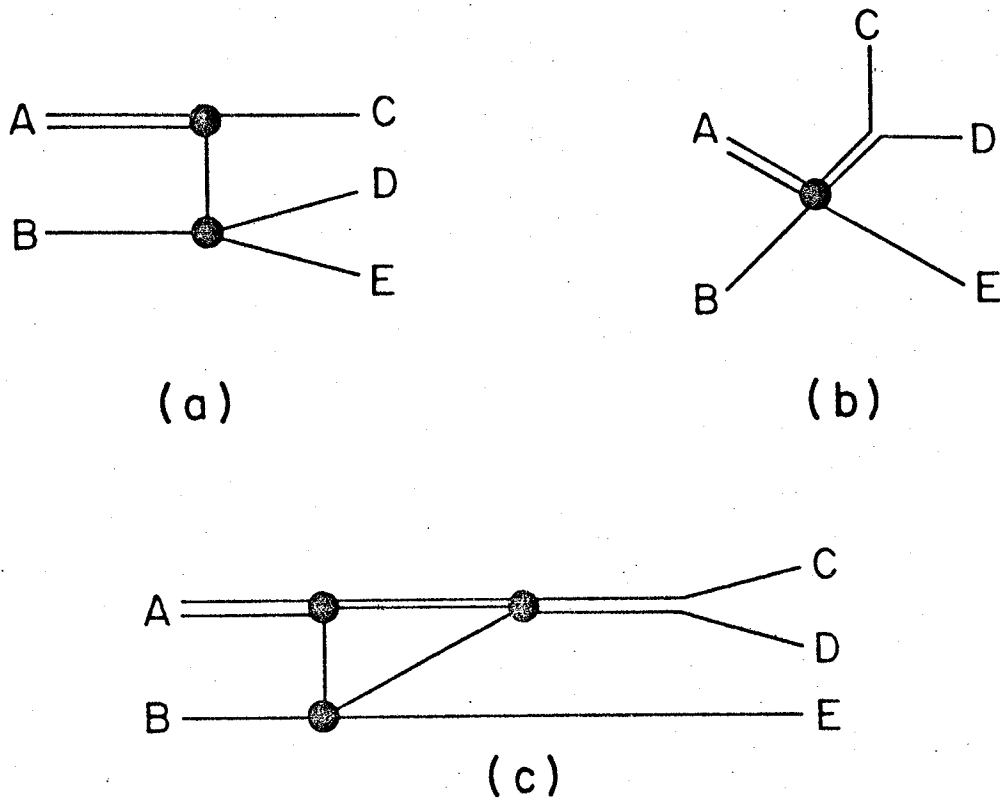


Figure 1.1 Feynman diagrams representing:  
(a) quasi-free scattering (QFS)  
(b) final state interaction (or sequential decay) (FSI)  
(c) the modification of quasi-free scattering by a final state interaction  
(after McKee, 1973)

Nakamura et al. (1978) who suggested that a three-body theory applied to the deuteron breakup on alpha particles might describe the system more successfully.

At the same time Koike (1978a) has reported a Faddeev type formulation of  $(d + \alpha)$  elastic scattering. This author solves the Amado-Lovelace equations along lines briefly described in section (1.2) of this chapter, predicts phase shifts which are in reasonable accord with experimentally determined phase shifts and the properties of the  ${}^6\text{Li } 1^+$  state. Charnomordic et al. (1977) have investigated the  ${}^6\text{Li}$  aspect of the  $(d + \alpha)$  system in detail and confirm the validity of the three-body approach. The results of their calculations for  $(d + \alpha)$  elastic scattering are in good agreement with experimental data as far as the cross-sections go. Qualitative agreement between theory and experiment results as far as vector analysing powers are concerned. The success of the model is limited in describing the tensor polarisation observables in  $(d + \alpha)$  elastic scattering.

Koike (1978b) has extended the three-body model for  $(d + \alpha)$  elastic scattering to the case of the  $(n + p + \alpha)$  final state. The predictions are in general agreement with the experimental data at an alpha particle bombarding energy of  $E_\alpha = 15$  MeV (results of Koersner et al., 1977) and  $E_\alpha = 42$  MeV (results of Warner and Bercaw, 1968). In these calculations the  ${}^2\text{H}(\alpha, \alpha p)n$  is studied and the results reproduce the experimental cross sections. The agreement is especially good when final state interactions of the  $N-\alpha$  and  $n-p$  are taken into account.

As far as the  $1^+$  resonance in  ${}^6\text{Li}$  is concerned, the model of Koike (1978b) has been compared to the results of Dasgupta et al. (1980). The experimental results cover the energy range  $9.735 \text{ MeV} < E_\alpha < 11.3 \text{ MeV}$ . These authors, in their study of the  ${}^2\text{H}(\alpha, p\alpha)n$  reaction, report qualitative agreement with three-body calculations.

The three-body model has also been applied to the kinematically incomplete reaction  ${}^4\text{He}(\vec{d}, p){}^4\text{He}$  (Koike, 1980). The aim was to investigate the role of the decay process from the  $1^+$  resonance of  ${}^6\text{Li}$ , since it was felt that this is important in a rather wide energy region, and most pronounced in the vicinity of the  $n$ - ${}^4\text{He}$  final state interaction peak (or  ${}^5\text{He}_{g.s.}$ ). The theoretical model, as briefly outlined in section (1.2), has been applied to this reaction and, here again, good agreement results with the cross-section data of Nakamura et al. (1978), although not at proton laboratory angles larger than  $40^\circ$ . The analysing powers are also reproduced well by this model. The model also predicts the data of Keller and Haeberli (1971) at 11 MeV incident deuteron energy, Ohlsen and Young (1964) at  $E_d=11 \text{ MeV}$  and Kambara et al. (1978) at  $E_d = 7.8 \text{ MeV}$ . The model also has been successful in predicting the neutron double differential cross-section ( $d^2\sigma_n/dE_n d\Omega_n$ ) and neutron polarisation at an incident  $\alpha$ -particle energy of 39.4 MeV in the study of the  ${}^2\text{H}(\alpha, \vec{n})p$   ${}^4\text{He}$  reaction (Knox et al., 1975) and predicts these quantities at the  ${}^5\text{Li}_{g.s.}$  rather well. Agreement is also good when the model is applied to the results of the kinematically complete experiment of Oswald et al. (1981) in which the authors report triple scattering cross sections and analysing powers of the reaction  ${}^4\text{He}(\vec{d}, p\alpha)n$  at  $E_d = 18 \text{ MeV}$ .

Faced with this success, Koike (1980) has applied the model to the calculation of deuteron tensor polarisation observables ( $T_{20}$ ,  $T_{21}$  and  $T_{22}$ ) of the reaction  ${}^4\text{He}(\vec{d}, p){}^4\text{He}$  at  $E_d = 15$  MeV. The model as it stands has no n-p tensor force included in the interaction.

Very recently Ishikawa et al. (1982) have published angular distributions of the polarisation observables ( $T_{20}$ ,  $T_{21}$ ,  $T_{22}$ ) in the  ${}^4\text{He}(\vec{d}, p){}^4\text{He}$  reaction at  $E_d = 12$  and 21 MeV at the final state interaction corresponding to the  ${}^5\text{He}_{g.s.}$ . The agreement with the predictions of the model of Koike (1980) is very poor. Neither the shapes nor the magnitudes of the experimental data are reproduced by the theory. Furthermore, there are no deuteron tensor analysing powers reported in the literature as a function of proton energy. In view of the success of the model and realisation of its limitations we have set out to determine the deuteron tensor analysing power ( $A_{yy}$ ) in the reaction  ${}^4\text{He}(\vec{d}, p){}^4\text{He}$  and, at the same time, the deuteron vector analysing power ( $A_y$ ). The latter is known to agree qualitatively with the results of the model (Koike, 1980) and is expected to serve as a basis for comparison.

In the next section some of the important aspects of the theoretical formulation of the deuteron-alpha system as a three-body problem are considered. Section (1.3) is devoted to the description of the experiment. The results are discussed in section (1.4). Some suggestions and recommendations for further work are made in section (1.5) of this chapter. These are believed to be helpful in contributing toward the understanding of the deuteron-alpha system in particular and the three-body model approach used to describe it.

## 1.2 THEORY

An attempt is made in this section to discuss, in a qualitative manner, the theoretical background to the formulation of the deuteron-alpha system as a three-body problem. A detailed treatment of the subject is due to Koike (1978a, 1978b, 1980). The discussion presented here is based on the contents of these papers. Its purpose is to present the salient features of the theory in order to understand and interpret the results of the experimental work reported in section (1.3) of this chapter. The observables of interest are defined. This is followed by a simplified discussion of the interaction used to describe the deuteron-alpha system. An explicit reference is made to the approximations made in the theory and their relevance to the present investigation. A few comments are included with regard to the method of solving equations describing the system and the values of the parameters used in the calculations of Koike (1980) with which the experimental results of the present work are compared. A useful reminder here regarding notation is in order. The Madison convention (1971) is adhered to throughout this chapter.

An observable "O" is given, according to quantum mechanics as the eigenvalue of the operator " $\hat{O}$ " which operates on the state  $|i\rangle$  describing the system. This is expressed formally as:

$$O = \langle i | \hat{O} | i \rangle \quad \dots(1.3)$$

In M-matrix terminology this is written as:

$$O = \frac{\int d\hat{x}_i \text{Tr}\{\hat{M}O\hat{M}^\dagger\}}{\int d\hat{x}_i \text{Tr}\{M\hat{M}^\dagger\}} \quad \dots(1.4)$$

$x_i$  in equation (1.4) expresses the set of variables over which the integral is carried out.

The observables of interest here are the deuteron vector and tensor analysing powers ( $A_y$  and  $A_{yy}$ ) of the reaction  ${}^4\text{He}(\vec{d}, p){}^4\text{He}$ . Applying equation (1.4) one obtains:

$$A_y = \frac{\int d\hat{p} \text{Tr}\{M S_y M^\dagger\}}{\int d\hat{p} \text{Tr}\{M M^\dagger\}} \quad \dots(1.5)$$

$A_{yy}$  is obtained from the relation (Ohlsen, 1975):

$$A_{yy} = -\sqrt{3} T_{22} - \frac{1}{\sqrt{2}} T_{20} \quad \dots(1.6)$$

which leads to (Ohlsen, 1972):

$$A_{yy} = \frac{\int d\hat{p} \text{Tr}\{M(3S_y^2 - 2)M^\dagger\}}{\int d\hat{p} \text{Tr}\{M M^\dagger\}} \quad \dots(1.7)$$

where  $S_y$  is the y-component of the spin-1 angular momentum operator.  $\hat{p}$  is the momentum of the  $\alpha$ -particle relative to the neutron.

The potential set used to describe the system is a one-term separable potential with a Yamaguchi-type form factor in each partial wave of the two-body subsystem,

$$v_{\gamma\ell j}(p, p') = \lambda_{\gamma\ell j} g_{\gamma\ell j}(p) g_{\gamma\ell j}(p') \quad \dots(1.8)$$

with

$$g_{\gamma\ell j}(p) = p^\ell / (p^2 + \beta_{\gamma\ell j}^2)^{\ell+1} \quad \dots(1.9)$$

$\lambda$  is the strength of the interaction in a particular channel.  $\gamma$  defines the reaction channel in the following manner:

$$\gamma = \begin{cases} 1 & \text{for the n-p interaction} \\ 2 & \text{for the } \alpha\text{-N interaction} \end{cases} \quad \dots(1.10)$$

It will be seen very shortly how this assignment arises.  $\ell$  and  $j$  are the orbital and total angular momentum respectively.  $p$  and  $p'$  refer to the relative momenta in the resulting two-body subsystems.  $\beta$  is the effective range. It is appropriate to state explicitly the reaction channels:

$$d + \alpha \rightarrow \begin{cases} \alpha + (p,n) \\ p + (n,\alpha) \\ n + (\alpha,p) \end{cases} \quad \dots(1.11)$$

where the brackets indicate the two particles that interact in the final state. It is easy to see how the values of  $\gamma$  are assigned in equation (1.10) since the second and third channels of equation (1.11) are identical except for isospin.

It is clear from equation (1.11) that the  $(d + \alpha)$  system may be approached along the lines of a three-body system. A modified potential set of CPV-A type (Cattapan et al., 1975) is used for the  $p_{3/2}$ ,  $p_{1/2}$  and  $s_{1/2}$  waves of the N- $\alpha$  interaction. This potential has essentially been stated in equation (1.8). Its details may be found in the references cited. The numerical values of the parameters used to predict the observables of interest here (as defined by equations 1.5 and 1.7) are given in table I of Koike (1978b). It should be remarked that the parameters used for the  $p_{1/2}$  partial wave are different to those used by Cattapan et al. (1975). The parameters used by Koike (1978b) predict the experimental  $p_{1/2}$  partial wave phase shifts for

$n$ - $\alpha$  elastic scattering of Arndt and Roper (1973) excellently all the way up to a neutron energy of approximately 20 MeV, while the parameter set of Cattapan et al. (1975) fails above a neutron energy of 3 MeV. In the  $p_{3/2}$  and  $s_{1/2}$  partial waves, however, the parameters of Cattapan et al. (1975) are still in good agreement with experimentally determined results (Arndt et al., 1973).

For the two nucleon interaction a triplet s-wave potential is used. A modification due to the Coulomb interaction is included approximately. There is no tensor force in the theoretical formulation of the problem. As a result all polarisation effects are caused only by the difference of the potential between  $p_{3/2}$  and  $p_{1/2}$  waves, or in more common terminology the spin-orbit force in the  $N$ - $\alpha$  interaction. The exclusion of the tensor force is particularly interesting in the context of the data obtained in the present work and will be discussed in sections (1.4) and (1.5).

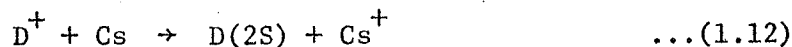
Koike (1980) solves the Amado-Lovelace equations, with the input as described briefly in this section, using the Padé approximant method. The results of his calculations are compared with the experimental data in a manner reported in the introduction to this chapter. Of particular significance are the results of Ishikawa et al. (1982). It will be seen in section (1.4) that  $A_{yy}$  values calculated according to equation (1.6) from values of  $T_{20}$  and  $T_{22}$ , reported by Koike (1980), do not agree with results obtained experimentally. The source of the disagreement, its significance and interpretation will be discussed in section (1.4).

### 1.3 EXPERIMENT

#### 1.3.1 The Deuteron Beam:

A Lamb-Shift source of the nuclear spin filter type is used to produce the polarised deuteron beam. The theory, operation and construction of this type of source is amply covered in numerous articles (see for example Clegg, 1971). More specifically, the University of Manitoba polarised ion source is discussed in great detail by de Jong (1981). The intention here is to outline the production and acceleration of the polarised deuteron beam used in the present study. The remainder of the discussion relating to the ion source is a summary of de Jong (1981).

$D^+$  ions are generated in a duoplasmatron ion source. They are extracted with an accel-decel system which accelerates them to 10 keV then decelerates them to 1.1 keV.  $D^+$  ions then enter a Cs canal where the following reaction takes place:



The neutral D atoms in the metastable 2S state have a different energy than the  $D^+$  ions. This is achieved by biasing the Cs cell above ground to an appropriately chosen voltage.

The neutral particles that are in the 2S state (~20%) are polarised by passing them through the spin filter. Unwanted spin states are selectively returned to the ground state, leaving only the atoms with the desired spin state in the metastable 2S state.

Deuterium atoms are ionised in argon gas by the charge exchange reaction:



The deuterium atoms in the metastable 2S state have just the right energy required for the removal of an electron from argon atoms while neutral deuterium atoms in the ground state do not, thus metastable atoms are selectively ionized.

Upon entrance to the acceleration system the ions are first decelerated. Those ions which originated in the Cs cell are repelled while those formed in the argon cell have sufficient energy to pass through the decel electrode. The latter ions are highly polarised. They are accelerated to 11 keV and injected into the cyclotron.

The University of Manitoba cyclotron is a sector-focused isochronous cyclotron. It accelerates protons to energies between 20 and 50 MeV and deuterons to energies between 12 and 24 MeV. The  $D^-$  beam is axially injected into the cyclotron and accelerated to an energy of 15 MeV. It is stripped of its two electrons with the aid of an aluminium foil. The emerging deuteron beam is then deflected by  $45^\circ$  by a bending magnet and strikes a target of  $^4\text{He}$  gas contained in a gas cell of diameter 6 cm. The gas is under a pressure of one atmosphere (14.2 p.s.i.). The energy of the deuteron beam at the centre of the target is 14.8 MeV. The beam is collected in a Faraday cup downstream from the scattering chamber and the charge is integrated in the usual manner. The cyclotron beam line layout is depicted in figure (1.2).

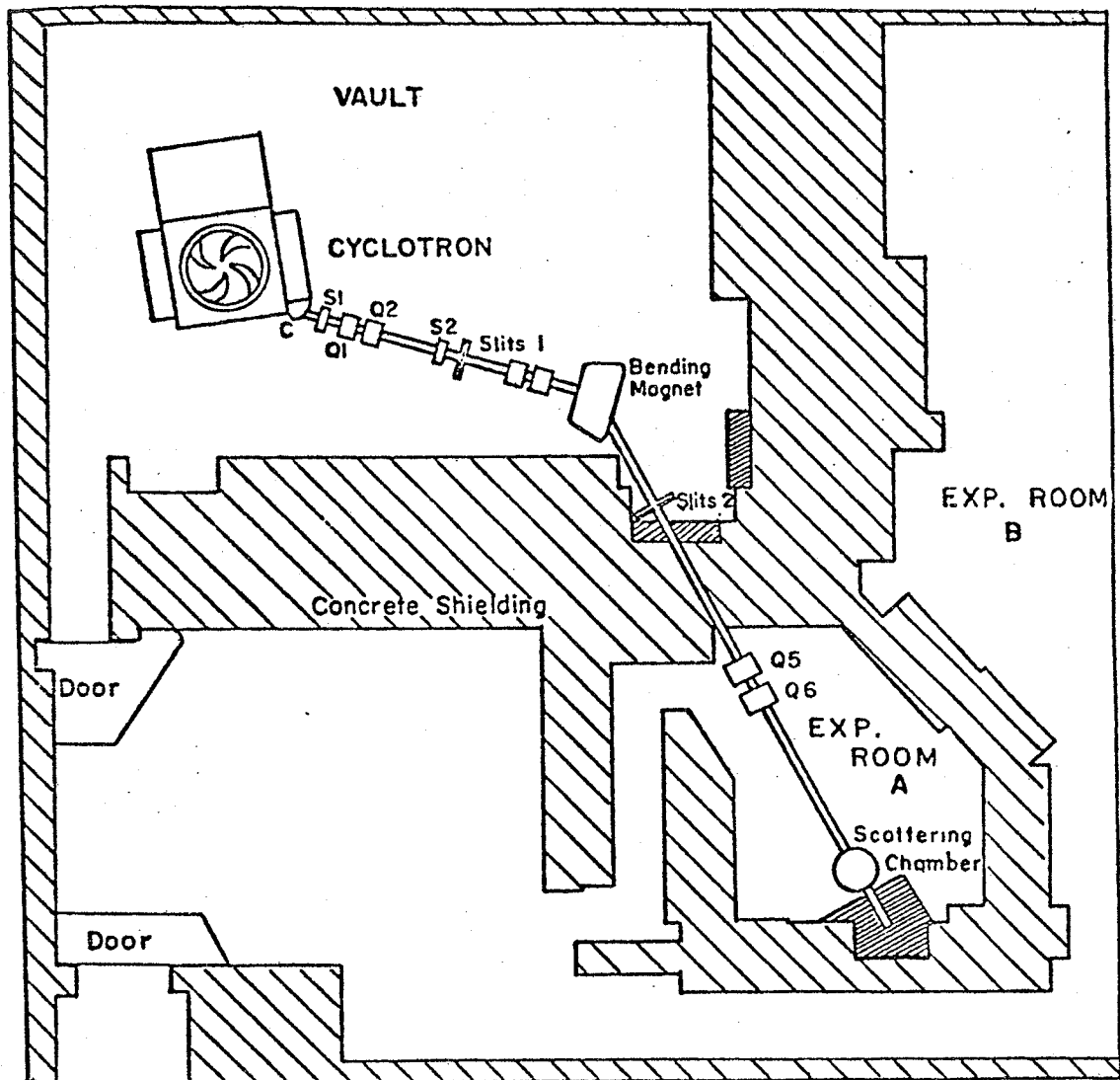


Figure 1.2 Cyclotron Beam Line Layout.

During the course of these experiments the beam polarisation was typically 70% for the vector polarised beam and -1.4 for the tensor polarised beam. Beam current on target was typically 100 pA.

Beam optics was initially set with the beam polarisation turned off in order to obtain a sufficiently intense deuteron beam which can be viewed on a fluorescent screen at the position of the target centre. When the polarisation is turned on again, beam centering was achieved by maximising the Faraday cup current.

### 1.3.2 Experimental Setup:

The apparatus consists of a conventional scattering chamber 71 cm in diameter at the centre of which a gas cell is situated. The gas cell is 6 cm in diameter with a Kapton entrance window of 1 cm diameter. Helium gas is introduced into the cell through a feedline connected to a pressure gauge. The pressure in the target is monitored continuously throughout the experiment and remained at one atmosphere (14.2 p.s.i.) to within  $\pm 1.4\%$  ( $\pm 0.2$  p.s.i.). The gas cell is flushed at regular intervals in order to avoid possible contamination with air.

The detection system consists of silicon surface-barrier detectors of 100  $\mu\text{m}$   $\Delta E$  (passing) and a 2 mm E (stopping) in thickness comprising a  $\Delta E$ -E particle identification telescope. Electronic processing of the signals from the experiment is discussed in the following subsection (1.3.3). Telescopes were placed to the left and right of the direction of propagation of the beam. A set of two collimators were placed in front of each telescope. The geometrical parameters of the collimation

Table 1.1 Geometrical parameters of the collimation system used in the  ${}^4\text{He}(\vec{d},p){}^4\text{He}$  reaction experiment.

|   | <u>Width</u>             | <u>Height</u>        |
|---|--------------------------|----------------------|
| Front collimator                                | $(3.29 \pm .01)$ mm      | $(12.81 \pm .01)$ mm |
| Back collimator                                 | $(2.63 \pm .01)$ mm      | $(12.74 \pm .03)$ mm |
| Distance of target centre from front collimator | $(151.6 \pm .8)$ mm      |                      |
| Intercollimator distance                        | $(156.4 \pm .8)$ mm      |                      |
| Full width resolution of the detection system   | $(1.24 \pm .01)$ degrees |                      |

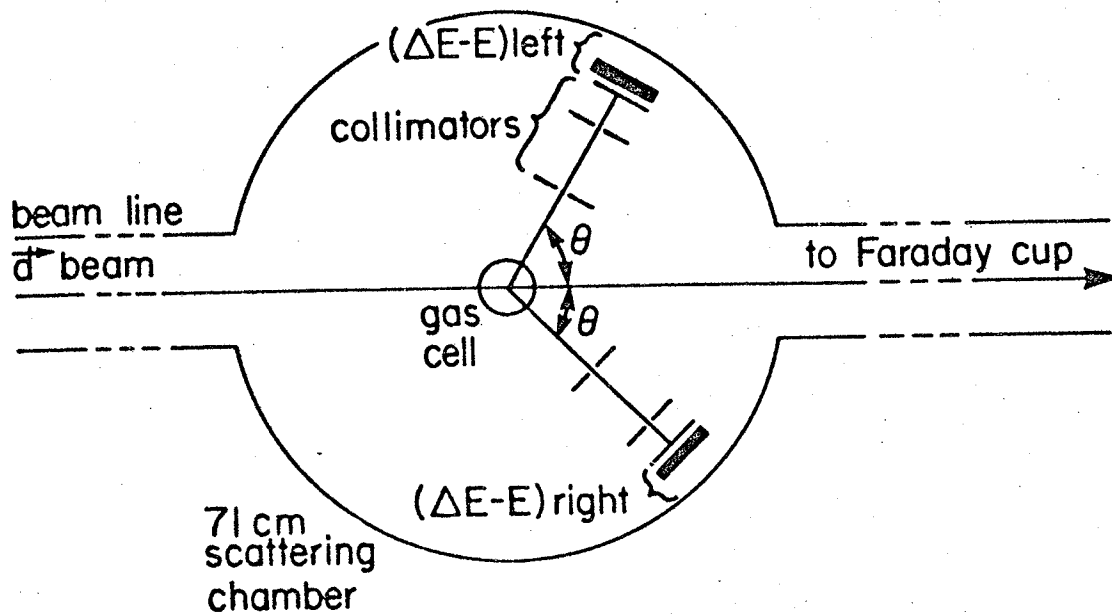


Figure 1.3 Diagram of experimental setup used for measurement of deuteron vector and tensor analysing powers ( $A_y$  and  $A_{yy}$ ) in  ${}^4\text{He}(\vec{d},p){}^4\text{He}$  reaction (not to scale).

system are presented in table (1.1). The experimental setup is sketched in figure (1.3).

### 1.3.3 Electronics:

The electronic circuit used is shown in figure (1.4). It is a standard  $\Delta E$ -E particle identification telescope circuit. Signals from each detector of both telescopes pass through a preamplifier and are then transferred to the cyclotron control room where they are fed to a spectroscopy amplifier. The bipolar output of the spectroscopy amplifier forms the input of the timing single-channel analyser (TSCA). The positive signal from the TSCA is fed to a coincidence unit whose output is used to gate the linear signals arriving at the linear gate and stretchers.

Unipolar signals from the  $\Delta E$  and E spectroscopy amplifiers are summed with the aid of a dual sum and invert module and passed through a linear gate and stretcher, an analogue to digital converter and then to a PDP15/20 computer. This signal corresponds to the total energy of the detected particles, and is marked  $E_{TOT}$  in figure (1.4).

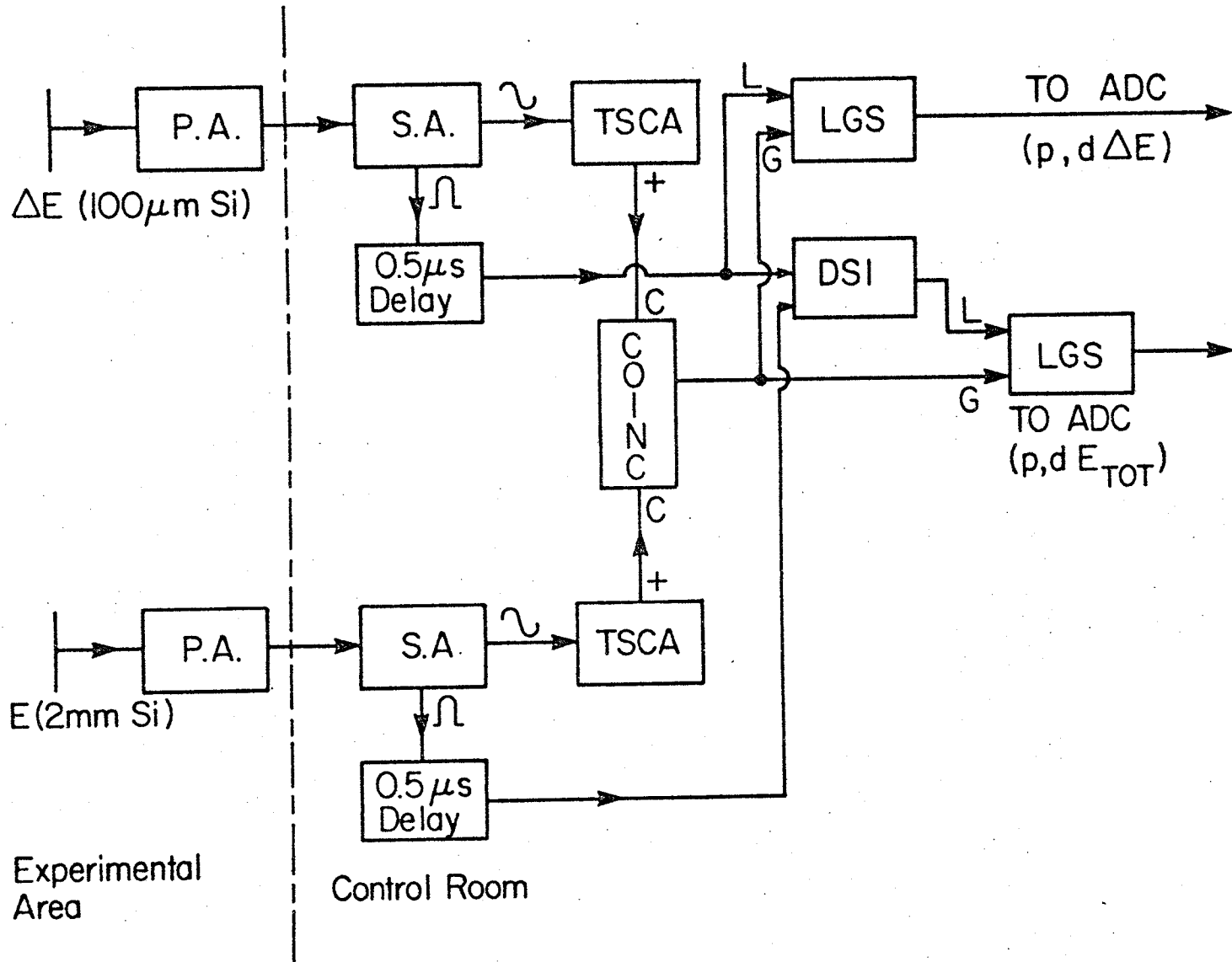
The linear signal from the  $\Delta E$  spectroscopy amplifier is fed directly to a linear gate and stretcher which is gated by the coincidence unit. The output feeds an analogue to digital converter and a PDP15/20 computer. This is marked  $\Delta E$  in figure (1.4).

An in-house data acquisition program named XMIRAD was used to accumulate  $\Delta E$ -E events from each detector and display the data in the form of two-dimensional scatter plots. Software windows were then

Figure 1.4  $\Delta E$ -E particle identification telescope

P.A.: preamplifier (ORTEC 109A), S.A.: spectroscopy amplifier (ORTEC 455), DSI: dual sum and invert (ORTEC 443A), COINC: coincidence unit, LGS: linear gate and stretcher (ORTEC 442), ADC: analogue-to-digital converter.

Figure 1.4



drawn to select proton and deuteron events and route them to different regions of the data files. Data was logged on tape and histograms in the form of 1024 channel binary files are stored on tape for offline analysis.

#### 1.3.4 Procedure:

The deuteron beam bombarded the  $^4\text{He}$  target in runs with spin up, spin down and tensor polarised ( $m=\pm 1, 0$ ) beam. Particulars relating to the deuteron beam and the apparatus have been discussed in subsections (1.3.1) and (1.3.2) earlier.

Beam polarisation was measured before, during and after each run by means of the quench ratio technique. This technique is outlined in detail elsewhere (de Jong, 1981). It has proven to be a reliable means of determining beam polarisation. To support this statement Birchall et al. (1980) have measured vector and tensor analysing powers of elastically scattered deuterons from  $^4\text{He}$  at 12.6 MeV incident deuteron energy using the same facilities used in the present experiment. Their results are in excellent agreement with the data of Schmelzbach et al. (1976).

Proton spectra from the reaction  $^4\text{He}(\vec{d}, p)n^4\text{He}$  were obtained at proton laboratory angles of  $20^\circ$ ,  $30^\circ$ ,  $35^\circ$  and  $40^\circ$  for each of the three spin states of the incident deuteron beam. A typical spectrum is shown in figure (1.5) for a proton laboratory angle of  $30^\circ$ . The asymmetry between spin "up" and spin "down" is larger than that indicated in the figure by a factor of 1.45 which is the ratio of the total charge deposited on target in each run corrected for the beam

Figure 1.5 Proton spectra in the "left" detector from the reaction  ${}^4\text{He}(\vec{d},p)n{}^4\text{He}$  at  $E_d = 14.8$  MeV and proton laboratory angle ( $\theta_p^{\text{lab}}$ ) of  $30^\circ$ . The crosses are with the deuteron beam spin "up", polarisation 75% and total charge on target of  $3.12 \mu\text{C}$ . The continuous histogram is for deuteron beam spin "down", polarisation 79% and total charge of  $2.27 \mu\text{C}$ .

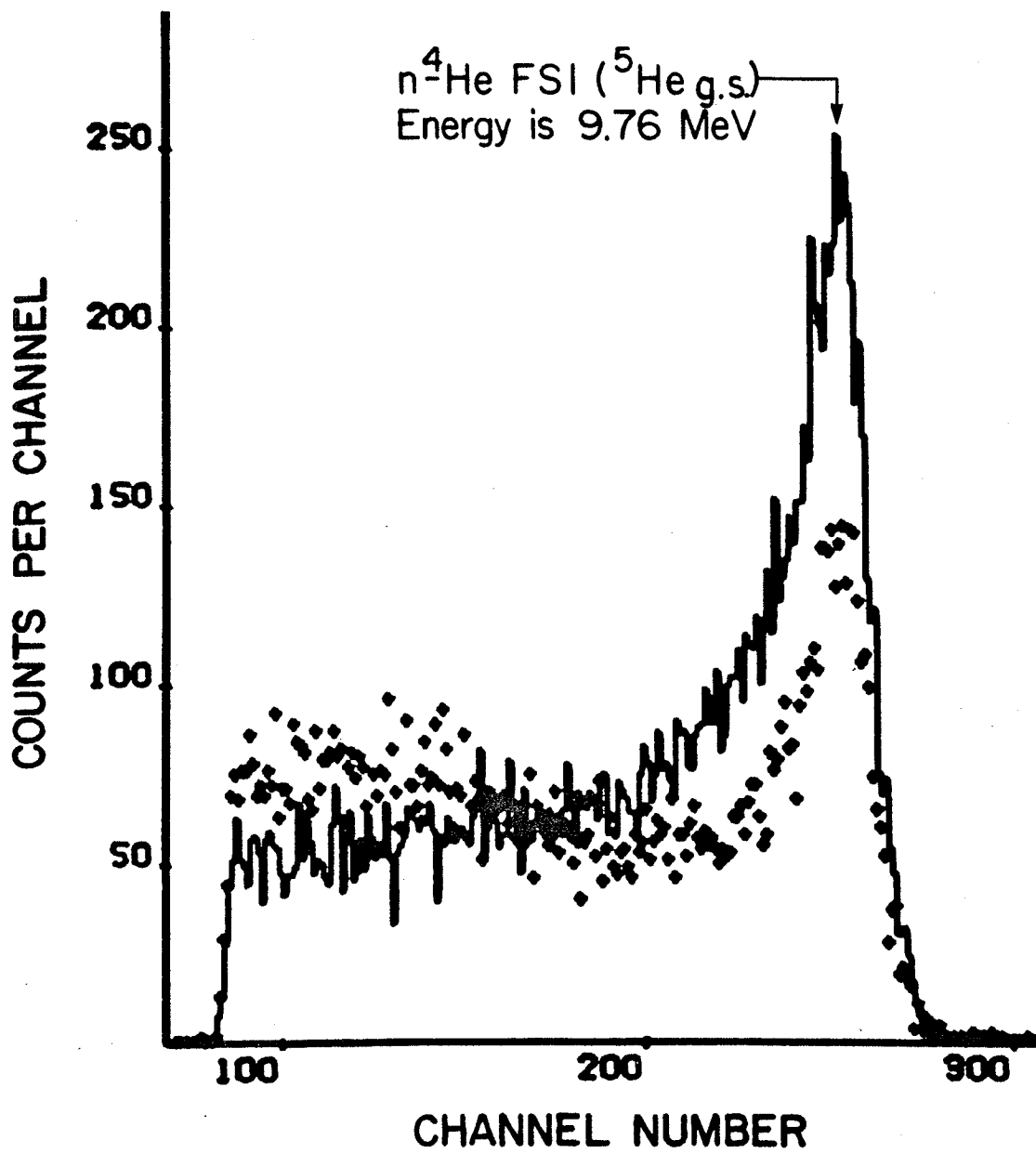


Figure 1.5

polarisation difference. The peaks at the high energy edge of the spectra correspond to the  $n$ - ${}^4\text{He}$  final state interaction peak (or  ${}^5\text{He}_{g.s.}$ ). The method of arriving at the energy of the FSI peak is discussed later in subsection (1.3.5) relating to data analysis.

Elastically scattered deuterons from  ${}^4\text{He}$  were also detected at the same laboratory angles at which proton measurements were carried out. From these data deuteron vector and tensor analysing powers were extracted in the usual way. The results obtained in this experiment are in reasonable agreement with the 15 MeV data reported by the Los Alamos group (Brown et al., 1979). The two sets of results for elastic scattering are tabulated in table (1.2). The agreement between them indicates that the system was functioning properly. Furthermore, they give credence to the claim made earlier relating to the reliability of the quench ratio technique in determining the beam polarisation.

The data of table (1.2) have also been used in correcting the tensor polarisation for any vector polarisation impurity that might be present in the  $m=0$  state of the beam. The manner in which this was carried out is described in Appendix A. The significance of this correction is discussed further in the subsection relating to the data analysis (1.3.5).

#### 1.3.5 Data Analysis:

Analysis of the data was carried out using the three spin state method of Ohlsen and Keaton (1973). The essentials of this method and

Table 1.2 Vector and tensor analysing powers ( $A_y$  and  $A_{yy}$ ) of elastically scattered polarised deuterons from  $^4\text{He}$ . The 15 MeV data are from Brown et al. (1979).

| $E_d$<br>$\theta^{\text{lab}}(^{\circ})$ | 14.8 MeV (This Work) |                 | 15 MeV (LASL Data) |                   |
|--|----------------------|-----------------|--------------------|-------------------|
|  | $A_y$                | $A_{yy}$        | $A_y$              | $A_{yy}$          |
| 20                                       | $-.013 \pm .07$      | $.068 \pm .13$  | -----              | -----             |
| 30                                       | $-.242 \pm .066$     | $.366 \pm .099$ | $-.2254 \pm .0065$ | $.2917 \pm .0083$ |
| 35                                       | $-.668 \pm .051$     | $.614 \pm .09$  | $-.7034 \pm .0082$ | $.516 \pm .012$   |
| 40                                       | $-.616 \pm .064$     | $.246 \pm .12$  | $-.6143 \pm .009$  | $.230 \pm .015$   |

its advantages are presently summarised. The reader is referred to the original paper for full details.

The yield in the left detector according to the three spin state method is given by equation (54) of Ohlsen and Keaton (1973). This is, with the notation appropriately modified to suit the present discussion:

$$\begin{aligned}
 L^+ &= n^+ N^+ \Omega_L E_L \sigma_o \left\{ 1 + \frac{3}{2} p_z^+ A_y + \frac{1}{2} p_{zz}^+ A_{yy} \right\} \\
 L^0 &= n^0 N^0 \Omega_L E_L \sigma_o \left\{ 1 + \frac{3}{2} p_z^0 A_y + \frac{1}{2} p_{zz}^0 A_{yy} \right\} \quad \dots(1.14) \\
 L^- &= n^- N^- \Omega_L E_L \sigma_o \left\{ 1 + \frac{3}{2} p_z^- A_y + \frac{1}{2} p_{zz}^- A_{yy} \right\}
 \end{aligned}$$

The "+, 0 and -" refer to spin up, tensor polarised beam and spin down respectively. Capital L's refer to the yield in the detector. n is the total charge deposited on target, N is the number of  $^4\text{He}$  atoms per  $\text{cm}^2$  in the target,  $\Omega$  the detector solid angle and E the efficiency of detection. Other symbols have their usual meanings. From equations (1.14) we can define  $\ell^+$  and  $\ell^-$  as follows:

$$\begin{aligned}
 \ell^+ &= \frac{L^+ n^0 N^0}{L^0 n^+ N^+} = \frac{1 + \frac{3}{2} p_z^+ A_y + \frac{1}{2} p_{zz}^+ A_{yy}}{1 + \frac{3}{2} p_z^0 A_y + \frac{1}{2} p_{zz}^0 A_{yy}} \\
 \ell^- &= \frac{L^- n^0 N^0}{N^0 n^- N^-} = \frac{1 + \frac{3}{2} p_z^- A_y + \frac{1}{2} p_{zz}^- A_{yy}}{1 + \frac{3}{2} p_z^0 A_y + \frac{1}{2} p_{zz}^0 A_{yy}} \quad \dots(1.15)
 \end{aligned}$$

Equations (1.15) demonstrate the advantage of the three spin state method. That is, the resulting observables are independent of the detector solid angle  $\Omega$  and the detector efficiency E. Therefore any errors resulting from these quantities are eliminated. Equations (1.15) are solved for  $A_y$  and  $A_{yy}$ :

$$A_y = - \left(\frac{2}{3}\right) \left(\frac{c_1 b_2 - c_2 b_1}{a_1 b_2 - b_1 a_2}\right) \quad \dots(1.16)$$

$$A_{yy} = - 2 \left(\frac{a_1 c_2 - c_1 a_2}{a_1 b_2 - b_1 a_2}\right)$$

with:

$$\begin{aligned} a_1 &= p_z^o \ell^+ - p_z^+ \\ a_2 &= p_z^o \ell^- - p_z^- \\ b_1 &= p_{zz}^o \ell^+ - p_{zz}^- \\ b_2 &= p_{zz}^o \ell^- - p_{zz}^- \\ c_1 &= \ell^+ - 1 \\ c_2 &= \ell^- - 1 \end{aligned} \quad \dots(1.17)$$

For the right detector an identical treatment holds except for a change in sign in the expression for  $A_y$  in equation (1.16) above. The availability of information from left and right detectors meant that any instrumental asymmetry due to beam wandering is properly taken into account by averaging over results obtained from both detectors in order to obtain the final result. Beam wandering, however, was not a problem in the present experiment as will become clear later in this subsection and in section (1.4). This is the second advantage of the approach employed here.

Beam polarisation is given by:

$$\begin{aligned} p_z^\pm &= \pm \left(1 - \frac{1}{Q}\right) \\ p_{zz}^\pm &= + \left(1 - \frac{1}{Q}\right) \end{aligned} \quad \dots(1.18)$$

for  $m = \pm 1$  state, that is "+" refers to spin up and "-" refers to spin down of the vector polarised beam. For the case of the tensor polarised beam ( $m = 0$  state), the vector and tensor polarisation ( $p_z^o$  and  $p_{zz}^o$  respectively) are given by:

$$p_z^o = \frac{1}{2} (1 - \delta^+) (1 - \frac{1}{Q})$$

$$p_{zz}^o = -\frac{1}{2} (1 + 3\delta^+) (1 - \frac{1}{Q}) \quad \dots(1.19)$$

$Q$  is the quench ratio mentioned earlier in §1.3.4.  $\delta^+$  is a correction which is necessary to incorporate in the case of the  $m = 0$  state. This is due to the fact that there is a vector polarisation component in the tensor polarised beam. The origin of this polarisation impurity is attributed to fringe field effects in the spin filter magnet (de Jong, 1981). Ideally  $\delta^+$  is unity, giving a  $p_{zz}^o$  of  $-2 (1 - \frac{1}{Q})$  and a  $p_z^o$  of zero, or a purely tensor polarised beam in the absence of fringe field effects of the spin filter magnet. This is not the case in practice, however, because of the finite length of the spin filter magnet. It was possible to extract  $\delta^+$  values from the  ${}^4\text{He}(\vec{d},d){}^4\text{He}$  analysing power data as has been briefly mentioned in §1.3.4. The reader is referred to appendix A for the method of obtaining  $\delta^+$  values. These have been incorporated into the data analysis in order to obtain correct values for the beam polarisation according to equation (1.19) above.

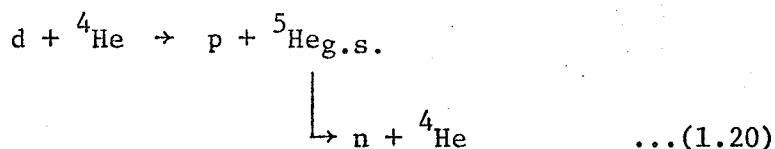
Having developed the relevant aspects of the three spin state method, it is now applied to the analysis of the data of the present experiment. In order to do that a data analysis program called POLCA was written (Smith, 1982). This is a command driven program which

reads in relevant regions in the data file and calculates the deuteron vector and tensor analysing powers ( $A_y$  and  $A_{yy}$ ) in accordance with the formalism developed earlier in this subsection. The way in which this is done is described presently.

Three data regions of proton spectra of the reaction  ${}^4\text{He}(\vec{d},p){}^4\text{He}$  corresponding to runs with spin up, spin down and tensor polarised beam per detector per angle are read into the program in the form of XMIRAD binary files, the same mode in which data were originally obtained during the course of the experiment. In addition to the spectra, the quench ratio for each particular run,  $\delta^+$  value and total charge on target are appropriately read in. The program deals with the information relating to each detector separately. It requests the energy calibration for each detector to be read in. This correctly converts the channel number, or abscissa, of the spectrum into the corresponding proton energy (in MeV). The method of arriving at the correct energy calibration is outlined shortly. The program then applies a gain matching factor to account for the fact that the left and right detectors have different gains. The way in which this is achieved is by requiring the positions of the final state interaction peak corresponding to the  ${}^5\text{He}_{\text{g.s.}}$  to be identical and correct for both detectors. This is easily done by imposing the requirement that the channels at which the number of counts is the greatest ( ${}^5\text{He}_{\text{g.s.}}$  peak) in spectra from both detectors coincide. The data are rebinned in 10 channel bins (approximately 400 keV).  $A_y$  and  $A_{yy}$  are then calculated from left and right detectors separately according to equation (1.16). The resulting analysing powers are then averaged and the final results are printed out.

In addition to calculating vector and tensor analysing powers, program POLCA determines the error on these quantities. The errors are due to counting statistics in this particular experiment. Because of the low count rate, due to low current on target, it would take an unreasonably long running time to improve on the present situation significantly. A 1% error due to beam current integration is also included. It is appropriate to note at this point that the results from the left and right detector were consistent within the experimental errors. This indicates that beam wandering or misalignment was not significant to be observed or reflected in the final results of the experiment. Further support of this statement is given in section (1.4) where the results of the experiment are examined.

The energy calibration was obtained by assigning the energy obtained from two-body kinematics to the high energy edge of the proton spectrum in the reaction:



The kinematic shift of this edge with angle gave a calibration which is independent of factors relating to the experimental setup. The value of the calibration obtained was 45 keV/channel. Nonlinearity in the calibration was of the order of 0.1%. The final state interaction peak corresponding to the  ${}^5\text{He}_{g.s.}$  was generally 20 channels (900 keV) below the high energy cut-off point of the proton spectrum. It is quite prominent (Figure 1.5) on the high energy shoulder of what would be otherwise a featureless phase-space

distribution. The values obtained for the energy at which the  ${}^5\text{He}_{\text{g.s.}}$  occurs are in good agreement with those reported by Koike (1980) for the  $20^\circ$  and  $40^\circ$  data validates the claim made earlier with regard to the adequacy of the energy calibration. There are no calculations in the position of the  ${}^5\text{He}_{\text{g.s.}}$  available at the present time for  $30^\circ$  and  $35^\circ$  proton laboratory angles to compare with. The evidence that the position of the  ${}^5\text{He}_{\text{g.s.}}$  is correct for these latter two angles comes from the shape of the deuteron vector analysing power which has a broad minimum in the region of the  ${}^5\text{He}_{\text{g.s.}}$ . This is discussed further in the next section.

The results of this experiment are presented in figures (1.6) and (1.7) and tabulated in appendix B. The significance of the results, their interpretation and the physics they convey are topics of the next section.

Figure 1.6 Deuteron vector analysing powers ( $A_y$ ) of  ${}^4\text{He}(\vec{d},p){}^4\text{He}$  reaction. Proton laboratory angles ( $\theta_p^{\text{lab}}$ ) are indicated.

$\bullet$  : data of present work  $E_d = 14.8$  MeV.  $20^\circ$  data are from the left detector only. Data at other angles are the average of left and right detector results.  $\blacktriangle$  : Nakamura et al. (1978) at  $E_d = 15$  MeV. —: results of three-body model calculations at  $E_d = 15$  MeV reported by Koike (1980). Position of the  $n$ - ${}^4\text{He}$  FSI peak ( ${}^5\text{He}_{g.s.}$ ) is at the minimum of the distribution. There are no other data nor calculations for  $\theta_p^{\text{lab}} = 30^\circ$  to compare with.

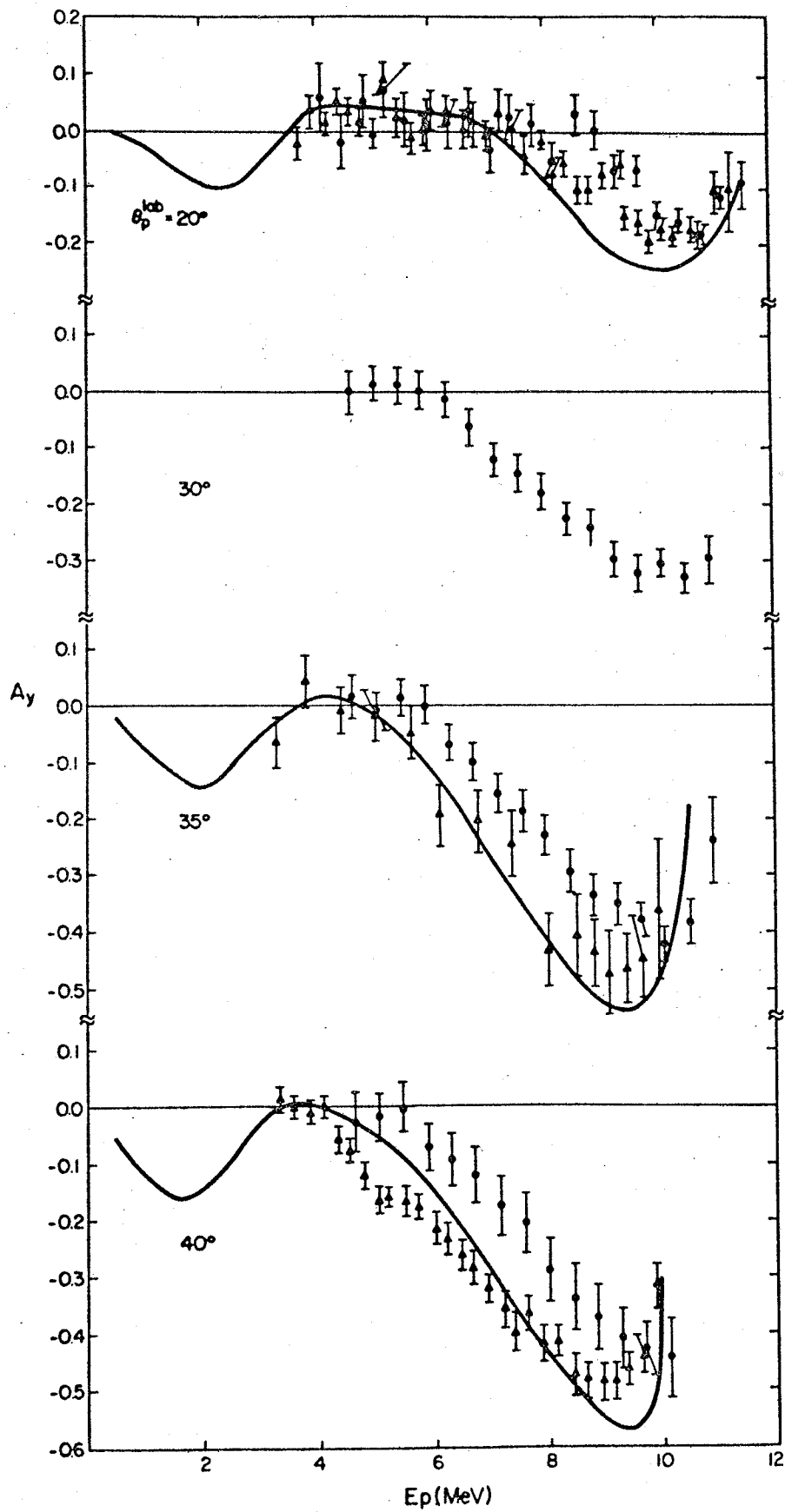


Figure 1.6

Figure 1.7 Deuteron tensor analysing powers ( $A_{yy}$ ) of  ${}^4\text{He}(\vec{d}, p){}^4\text{He}$  reaction. Proton laboratory angles ( $\theta_p^{\text{lab}}$ ) are indicated.

$\text{I}$ : data of present work at  $E_d = 14.8$  MeV.  $20^\circ$  data are from the left detector only. Data at other angles are the average of left and right detector results.

— : results of three-body model calculations from  $T_{20}$  and  $T_{22}$  at  $E_d = 15$  MeV reported by Koike (1980). The arrows refer to the position of the  $n$ - ${}^4\text{He}$  FSI peak ( ${}^5\text{He}_{\text{g.s.}}$ ). There is no published information at  $\theta_p^{\text{lab}} = 30^\circ$  and  $35^\circ$  to compare with data of present work.

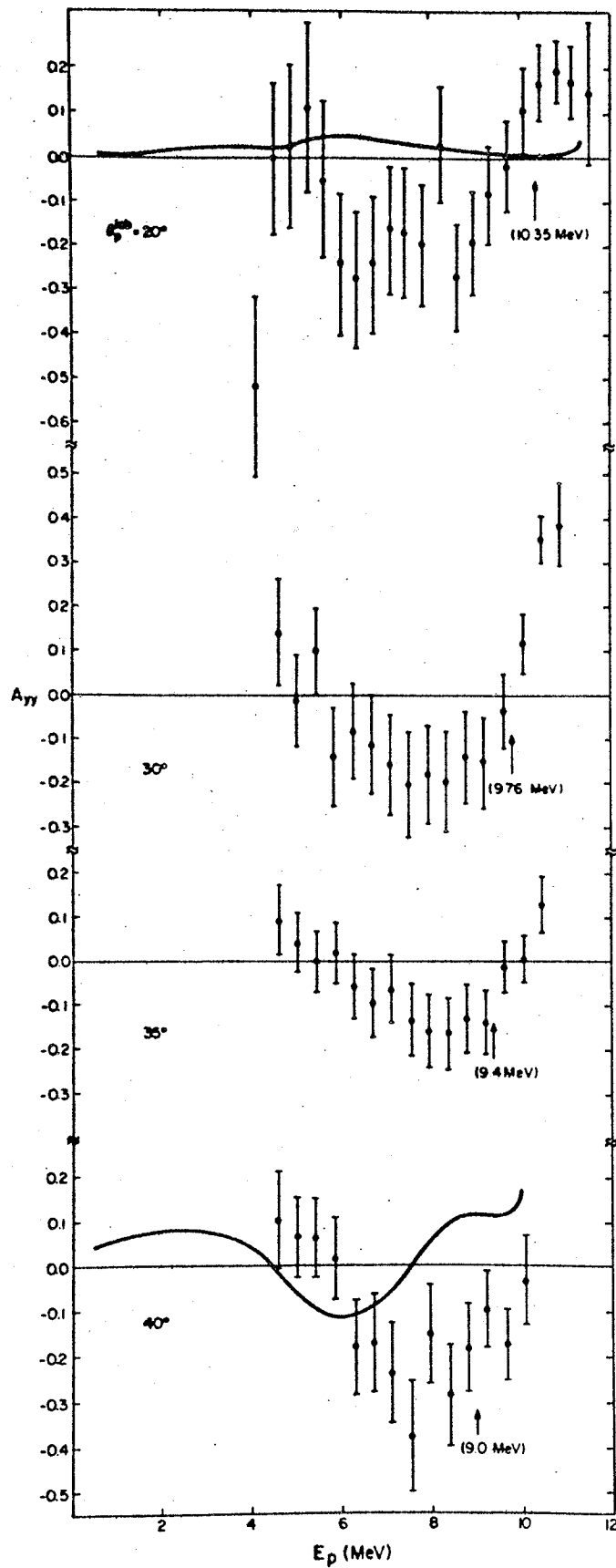


Figure 1.7

#### 1.4 RESULTS AND DISCUSSION\*

The deuteron vector analysing powers obtained in the present work are depicted in figure (1.6) for proton laboratory angles ( $\theta_p^{\text{lab}}$ ) of  $20^\circ$ ,  $30^\circ$ ,  $35^\circ$  and  $40^\circ$ . The data of Nakamura et al. (1978) and the calculations of Koike (1980) are also presented. At  $\theta_p^{\text{lab}} = 20^\circ$  the present results are in excellent agreement with those of Nakamura et al. (1978). The three-body model calculations of Koike (1980) predict the data fairly well, but overestimate the analysing power absolute value in the region of the  $^5\text{He}_{g.s.}$  (minimum of the distribution). There are no data to compare with present results for  $\theta_p^{\text{lab}} = 30^\circ$ . At  $\theta_p^{\text{lab}} = 35^\circ$  and  $40^\circ$ , here again the theory reproduces the data reasonably well thus affirming that the vector analysing power is adequately represented in the model and that it is sufficient to assume that polarisation effects result from the spin-orbit force in the N- $\alpha$  interaction as discussed in section (1.2).

A comment relating to the disagreement between the analysing power data reported in this experiment and the data of Nakamura et al. (1978) is in order. The disagreement at  $40^\circ$  laboratory angle may be regarded as significant. It is interesting to note that in section (2) of their paper, Nakamura et al. (1978) express some doubts relating to the energy calibration in the range of laboratory angles  $40^\circ$  to  $65^\circ$  employed in their experiment.

In figure (1.7) deuteron tensor analysing powers ( $A_{yy}$ ) of the  $^4\text{He}(\vec{d},p)n^4\text{He}$  reaction at  $E_d = 14.8$  MeV are reported for  $\theta_p^{\text{lab}} = 20^\circ$ ,  $30^\circ$ ,  $35^\circ$  and  $40^\circ$ . Together with these, theoretical predictions of  $A_{yy}$  values at  $E_d = 15$  MeV are presented. These are calculated at

---

\* See also Appendix C

from  $T_{22}$  and  $T_{20}$  values reported by Koike (1980) for  $\theta_p^{\text{lab}} = 20^\circ$  and  $40^\circ$  according to equation (1.6). There are no calculations at  $\theta_p^{\text{lab}} = 30^\circ$  and  $35^\circ$ . As far as the tensor analysing powers are concerned, a rather interesting picture emerges. The theoretical model predicts a positive  $A_{yy}$  at  $\theta_p^{\text{lab}} = 20^\circ$  over the entire proton energy range in complete contrast to experimentally determined values of  $A_{yy}$ . Furthermore, the model predicts rather low absolute values ( $< 0.05$ ), in disagreement with the experiment. At  $\theta_p^{\text{lab}} = 40^\circ$  the disagreement between theory and experiment persists, although a broad minimum in the calculated values of  $A_{yy}$  is seen. This, however, does not coincide with the experimentally obtained distribution of  $A_{yy}(E_p)$  in either magnitude or position. The minimum in  $A_{yy}$  seen at  $\theta_p^{\text{lab}} = 40^\circ$  is similar to that seen at  $30^\circ$ . There is consistency in behaviour amongst the four sets of data obtained, two of which are poorly represented by the three-body model. This disagreement is consistent with the findings of Ishikawa et al. (1982) at  $E_d = 12$  and  $21$  MeV as far as the  ${}^5\text{He}_{g.s.}$  is concerned, and goes beyond the position of the FSI to cover the entire proton distribution investigated. Possible sources of the discrepancy between theory and experiment and their physical significance are investigated in the remaining part of this section.

The first point one can make here is that the theoretical calculation does not include the tensor force. This has been referred to by Ishikawa et al. (1982). The need for the tensor force may be explained as follows. Since the deuteron is a loosely bound system, the  $\alpha$ -particle interacts with the neutron leaving the proton as a spectator. However, since the range of the deuteron wavefunction is

long, precisely because of the low binding energy, the role of the proton is not confined to that of a spectator. This argument was presented for the case of  ${}^2\text{H}(\alpha, p\alpha)n$  at  $E_\alpha = 140$  MeV by Lambert et al. (1982) in connection with the destructive interference between n-p FSI multiple scattering term and single scattering of the  $\alpha$ -p system in their study of quasi-free scattering. An n-p interaction of this type is angle dependent and is expected to be more significant at forward angles.

In view of the discussion above one can see how the three-body model would explain the vector analysing powers as being due to the spin-orbit force of the N- $\alpha$  interaction and fails to predict tensor polarisation observables. In terms of equations (1.5) and (1.7) discussed in section (1.2) earlier, one can "loosely" speak of  $A_y$  and  $A_{yy}$  as being "first order" and "second order" effects in the overall interaction that enters into the calculation.  $A_y$  is represented by the operator  $S_y$  while  $A_{yy}$  is represented by the operator  $(3S_y^2 - 2)$ . Each observable is sensitive to a particular term in the interaction. In this case the absence of the tensor force will justifiably predict theoretical results which do not correspond to experimentally determined quantities.

It is claimed in the literature that there is sensitivity to the percentage D-state in the deuteron wavefunction (e.g. Koike, 1980, 1978b). This might well be the case, however, there does not exist at the present time a calculation or an experiment which addresses this particular aspect of the problem directly for the  $(d + \alpha)$  system. In other words, the observables have not been examined theoretically with different values for the D-state as input, leaving other parameters

fixed.

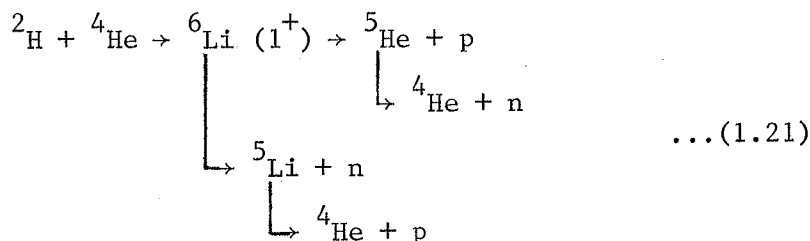
The only evidence available regarding the influence of the D-state probability in the deuteron wavefunction in this type of calculation comes from  $\vec{p}$ -d elastic scattering. Shimizu et al. (1982) have reported cross-sections and analysing powers at a proton energy of 64.8 MeV. The cross-sections they report are reproduced well by a YY0 P-D potential\* in the angular range  $40^\circ < \theta_{cm} < 120^\circ$ . The same potential reproduces the analysing power ( $A_y$ ) in the range  $80^\circ < \theta_{cm} < 130^\circ$ . YY0 P-D is a potential set with a Yamaguchi type separable potential and no  $^3S_1$ - $^3D_1$  coupling. When Coulomb effects are included this potential predicts the experimental cross-sections at forward angles too. It fails, however, to fit the analysing power data at back angles ( $130^\circ < \theta_{cm} < 170^\circ$ ). These are represented best by a YY7-P potential which contains separable potentials in  $^1S_0$ ,  $^3S_1$  -  $^3D_1$ , and all P-waves of the N-N interaction (Doleschall, 1973). The D-state in this potential is 7%. Koike et al. (1981) have studied the same reaction at a proton energy of 11.1 MeV. These authors find that the cross-sections are predicted equally well by YY4 and YY7 potentials, except at  $\theta_{cm} < 40^\circ$  where Coulomb effects dominate. The agreement between theory and experiment is less satisfactory when the theory is applied to the analysing power. The YY4 and YY7 potentials predict results which are almost identical everywhere and agree qualitatively with the overall shape of the analysing power.

---

\* The characters refer to the Yamaguchi form factor in the  $^1S_0$  state (Yamaguchi and Yamaguchi, 1954). The number gives the percentage D-state. Letters that follow the number refer to the partial waves included in the calculation.

As far as the influence of the deuteron D-state probability on the predictions of the three-body model of Koike (1980) is concerned, the information available is rather limited, with conflicting conclusions. The significance of D-state effects seem to have been overlooked with regard to the treatment of the  ${}^4\text{He}(\vec{d},p){}^4\text{He}$  reaction as a three-body system. A study of this aspect of the problem may yield valuable information.

It has been pointed out that the  $1^+$  state in  ${}^6\text{Li}$  (at 6.5 MeV) plays a significant role and exhibits three-body structure (Koike, 1980, 1978b) through the reaction mechanism:



The evidence in connection with this aspect of the  $(d + \alpha)$  system remains very limited. The cross-section reported in figure 9 of Koike (1980) for the  ${}^4\text{He}(\vec{d},p){}^4\text{He}$  reaction at 6.8 MeV is flat over the angle range  $60^\circ < \theta_p < 120^\circ$  c.m. and rather large. Direct experimental evidence reported by Dasgupta et al. (1980) is confined to the energy range of  $9.375 < E_\alpha < 11.30$  MeV. The agreement of the experimental results with theory is rather qualitative and a systematic experimental test is clearly necessary.

Finally, in summary, there are a variety of factors which enter into the theoretical description of the  $(d + \alpha)$  system as a three-body problem and it is necessary that the role of each of these be clearly



defined. In the present work, the experimental findings reported in figures (1.6) and (1.7) concentrate on a particular aspect of the overall problem, namely that of the ability of the three-body model to predict the deuteron tensor analysing powers ( $A_{yy}$ ) as functions of the proton energy. In view of the discussion that has already been presented, it is fair to say that the present experimental data are helpful in elaborating the successes and limitations of the three-body model reported by Koike (1980). Some suggestions for further work have already been implicitly made in this section. These and other suggestions are discussed further in the following section (§1.5).

### 1.5 FURTHER WORK

Much of the interest in the deuteron-alpha system as a three-body problem is rather recent. A three-body model is capable, in principle, of describing the  $(n + p + \alpha)$  final state and the approach has proved to be successful in predicting cross-sections and vector analysing powers in a variety of kinematic configurations. This is encouraging although the limitations of the model are not to be underestimated. A great deal of work is necessary, both theoretical and experimental, in order to disentangle the various components which enter into the description of the system. Some suggestions are made below.

There is a need to extend, and improve the quality of, the polarisation observables available on the  $(d + \alpha)$  system over a wider range of angles and energies. For that to be done the experimental requirements are higher beam intensity, rapid spin flip and continuous monitoring of the incident deuteron beam polarisation in a reaction of the type  ${}^4\text{He}(\vec{d}, p){}^4\text{He}$ . Particularly helpful will be the measurement of tensor polarisation observables. Ultimately, it will be necessary to measure all three tensor polarisation observables ( $T_{20}$ ,  $T_{21}$  and  $T_{22}$ ). This requires two more measurements, in addition to  $A_{yy}$ .

Experiments designed to investigate the role played by the D-state in the deuteron wavefunction are also helpful since this information will enable an appropriate representation of the n-p input in the three-body model.

As far as the contribution of the  $1^+(6.5 \text{ MeV})$  state in  ${}^6\text{Li}$  is

concerned, the information available on it is very limited. A suitably designed experiment at low incident deuteron energy, where this component of the system is most significant, may unambiguously determine any three-body behaviour that this state exhibits.

On the theoretical front, there is a pressing need to incorporate a n-p tensor force in the description of the  $(d + \alpha)$  system. This has been demonstrated in the experimental results reported in this work. The percentage D-state in the deuteron wavefunction and its influence on the observables needs to be systematically investigated. The energy range over which the  $1^+$  state in  ${}^6\text{Li}$  contributes significantly to the observables of the  $(d + \alpha)$  system needs to be clearly defined. The three-body behaviour that this state is claimed to exhibit remains unclear at the present time.

In conclusion, the success of the three-body model as it stands is interesting. The  $(d + \alpha)$  system is the simplest system involving a nucleus which can be studied as a three-body problem both theoretically and experimentally. It presents a variety of fronts on which the three-body force in nuclear physics might be tackled and promises a rich harvest for the theorist and experimentalist alike. Much work remains to be done.

CHAPTER TWO

SINGLE-PHOTON EMISSION FOLLOWING

PROTON-INDUCED DOUBLE K-SHELL

IONIZATION OF RUBIDIUM

## 2.1 INTRODUCTION

In ion-atom collisions, highly excited atomic states with several inner-shell vacancies may be produced through Coulomb excitation and other processes (Garcia et al., 1973). These processes can completely ionize the K-shell. The ionized atom usually returns to its ground state by the emission of two x-ray photons and (or) Auger electrons. An alternative mode of deexcitation of the doubly ionized K-shell is via the correlated transition of two electrons into the vacant K orbitals, with the subsequent emission of only one photon of approximately twice the K x-ray energy. The probability of occurrence of such a process is very small as will be seen later in this chapter. This phenomenon was first referred to by Heisenberg (1925).

Vinti (1932) carried out the first calculations of probabilities of single and double ionization. His efforts were directed to problems involving helium and helium-like ions. The model employed wavefunctions which are products of hydrogenlike wavefunctions, where the nuclear charge is replaced by a free parameter.

An important development in the area is the model of Gryzinski (1965). The model deals with the ion-atom interaction in terms of classical collision theory. It has been extended by McGuire and Richard (1973) to include the problem of multiple ionization. According to this model multiple ionization is a consequence of binary Coulombic collisions of charged particles and is dependent on the relative velocity of the projectile and orbital electron of the target atom. Furthermore, for the case of target bombardment by protons and heavy ions, the contribution to multiple ionization due to recoiling electrons

is believed to be negligible compared to multiple collisions of the incident particle.

The first systematic experimental investigation of the problem was carried out by Wölfli et al. (1975) and Stoller et al. (1977). These authors reported observation of x-rays due to two-electron one-photon transitions in Al-Al, O-Ca, Ca-Ca, Fe-Fe, Fe-Ni and Ni-Ni collisions. The cross-sections they measured were five times higher than the theoretical predictions. The discrepancy between theory and experiment was attributed to the fact that the theory was only true for the case of a fully stripped bombarding ion.

A somewhat different line of activity in the area was initiated by Gentry et al. (1976) who reported x-ray evidence suggesting the presence of element  $Z=126$  in monazite samples. In this connection it was believed that the observed x-ray transition could have included a contribution due to single-photon emission from rubidium which is naturally found in a mica environment in concentrations of up to 1000 ppm. Birchall et al. (1978), in a suitably designed experiment, have shown that the contribution could not have been significant. However, the upper limit obtained for the ratio of single-photon transition to double x-ray emission was a factor of 15 higher than the theoretical predictions based on the treatment of Gryzinski (1965) and employing the approximations suggested by McGuire and Richard (1973). Therefore the experiment did not constitute a test of multiple ionization theories.

Recently Isozumi (1980) reported the observation of two-electron one-photon transition in Mn following the K electron-capture decay of

$^{55}\text{Fe}$ . The results of this experiment are of the same order of magnitude as the predictions of classical collision theory. The radioactive decay process is not a collision process in the conventional sense. Radioactive decay via K electron capture ensures the creation of a single vacancy in the K-shell and may provide favourable conditions for the creation of a double vacancy. Therefore its description in terms of classical collision theory is questionable. Indeed this author has resorted to the model of Vinti (1932), alluded to earlier, to predict the probability of creation of a double vacancy in the K-shell. This model predicts results which are generally lower (by a factor of 1.25 to 2.75) than the experimentally measured  $(K_{\alpha\alpha}^h/K_{\alpha})$  ratio\*. This ratio is the probability of emission of x-rays due to two-electron one-photon transition  $(K_{\alpha\alpha}^h)$  divided by the probability of emission of a normal x-ray  $(K_{\alpha})$ .

The purpose of the present investigation is to test in detail the theory of multiple ionization as outlined in the works of Gryzinski (1965) and McGuire and Richard (1973). In the following section the impact parameter form of the theory, as detailed by McGuire and Richard (1973), will be used to express the ratio of double K-shell ionization cross-section to single ionization cross-section  $(\sigma_{2K}/\sigma_{1K})$ . Then the  $(K_{\alpha\alpha}^h/K_{\alpha})$  ratio, defined earlier will be calculated. Some numerical examples are given, on the basis of which an optimal set of criteria is chosen for an experimental test of the theory. This

---

\*Note that Isozumi's (1980)  $K_{\alpha\alpha}$  is our  $K_{\alpha\alpha}^h$ . The convention used here is of more widespread use.

experiment is reported in sections (2.3) and (2.4) of this chapter. Part of section (2.4) will deal with the data analysis and the extraction of a  $(K_{\alpha\alpha}^h/K_{\alpha})$  ratio. Finally, in section (2.5), our results are examined in the light of the theoretical considerations of section (2.2), compared with the available data and some conclusions are drawn.

## 2.2 THEORY

It is appropriate to start this section by examining the basic steps involved in the theoretical description of the process of double ionization followed by single-photon emission. The theory assumes that the projectile is a fully stripped ion. It makes two successive collisions (binary encounter) with the orbital electrons, thus creating a double vacancy. The collision process is depicted in figure (2.1). The double vacancy created is filled with two electrons from higher shells with the emission of two characteristic x-ray photons. There exists, however, a small but finite probability of the vacancy being filled by a correlated transition of two electrons, giving rise to the emission of a single photon. The calculation of the  $(K_{\alpha\alpha}^h/K_{\alpha})$  ratio, as defined in the introduction to this chapter, involves a determination of the probability that a double vacancy is created in the K-shell and that this excited state will decay via the emission of a single photon. These two steps are discussed separately below.

### 2.2.1 Double K-Shell Vacancy Production:

The ratio of the double vacancy production cross-section to that of single vacancy production ( $\sigma_{2K}/\sigma_{1K}$ ) is obtained by using equation (30) of McGuire and Richard (1973) and is:

$$\frac{\sigma_{2K}}{\sigma_{1K}} = \frac{\int P_K^2 \cdot 2\pi b db}{\int P_K (1 - P_K) \cdot 4\pi b db} \quad \dots(2.1)$$

b is the impact parameter and  $P_K$ , a function of b, is the probability of single ionization of the K-shell.

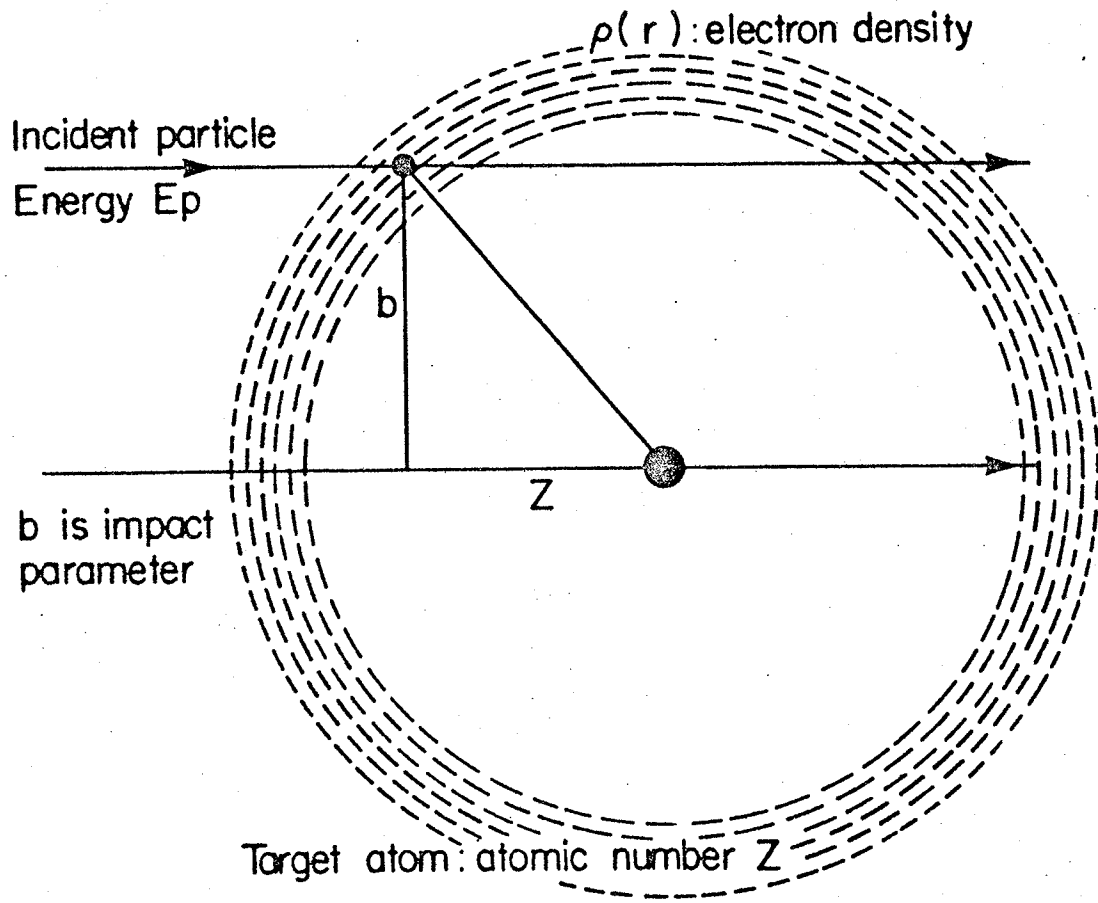


Figure 2.1 Ion-atom collision in the binary-encounter model. (After McGuire and Richard, 1973).

It is suggested by McGuire and Richard (1973) that the model of Kessel (Kessel and Rudd, 1970) successfully predicts the ionization probability. Applying this model to the particular case of the K-shell, one obtains:

$$\begin{aligned}
 P_K &\approx \sigma_{1K}/2\pi R^2 & b \leq R \\
 &= 0 & b > R
 \end{aligned}
 \dots(2.2)$$

Where  $R \leq (\sqrt{2} a_0/Z_K)$ .  $a_0$  is  $5.29 \times 10^{-2}$  nm and  $Z_K$  is the effective nuclear charge ( $Z-s$ ). Bethe and Salpeter (1957) have calculated  $s$  to be  $5/16$  for the K-shell. The equality sign holds when the velocity of the projectile is close to that of the orbital electron. Substituting equation (2.2) in (2.1) we obtain the result that,

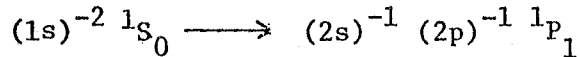
$$\frac{\sigma_{2K}}{\sigma_{1K}} = \frac{\sigma_{1K}}{2\pi R^2 - \sigma_{1K}}
 \dots(2.3)$$

Calculations based on equations (2.1) and (2.3) and an examination of their significance are discussed later in this chapter.

### 2.2.2 The Branching Ratio:

The next step in the calculation of the  $(K_{\alpha\alpha}^h/K_{\alpha})$  ratio is the determination of the probability that the double K-shell vacancy produced will be filled by a correlated transition giving rise to two photon emission. This quantity is called the branching ratio (B).  
 Oberg et al. (1976) have calculated this quantity by the Hartree-Fock method using a so-called "shake-down" model. This model deals with the allowed transitions on the basis of spin and parity conservation. The

two-electron single-photon transition is only allowed by the electric dipole transition:



The level diagram for this process and the competing process of hypersatellite ( $K_{\alpha}^h$ ) transitions is shown in figure (2.2). The model also takes into account the effect of the initial and final state configurations on the transitions. The branching ratio according to this model is given by:

$$B = \frac{P(K_{\alpha\alpha}^h)}{P(K_{\alpha}^h)} = \left( \frac{E_{\alpha\alpha}^h}{E_{\alpha}^h} \right)^3 \left( \frac{0.035}{Z^2} \right) \quad \dots(2.4)$$

where  $E_{\alpha\alpha}^h$  and  $E_{\alpha}^h$  are the single-photon and the hyper x-ray energies respectively. These are given by:

$$E_{\alpha\alpha}^h = 2E_{\alpha} + \Delta E_s \quad \dots(2.5)$$

$$E_{\alpha}^h = E_{\alpha} + \Delta E_s \quad \dots(2.6)$$

where  $E_{\alpha}$  is the  $K_{\alpha}$  x-ray energy and  $\Delta E_s$  is the energy shift due to screening and is given by:

$$\Delta E_s = 10.2 [Z^2 - (Z-s)^2] \quad \dots(2.7)$$

$s$  is the screening parameter defined earlier.  $E_{\alpha\alpha}^h$  and  $E_{\alpha}^h$  have been calculated by various authors (e.g. Wölfli and Betz, 1976 and Briand, 1976) and agree well with the experimental values obtained by Wölfli et al. (1975).

The  $(K_{\alpha\alpha}^h/K_{\alpha}^h)$  ratio is the product of equations (2.3) and (2.4) if the approximation of Kessel is employed, while it is the product of

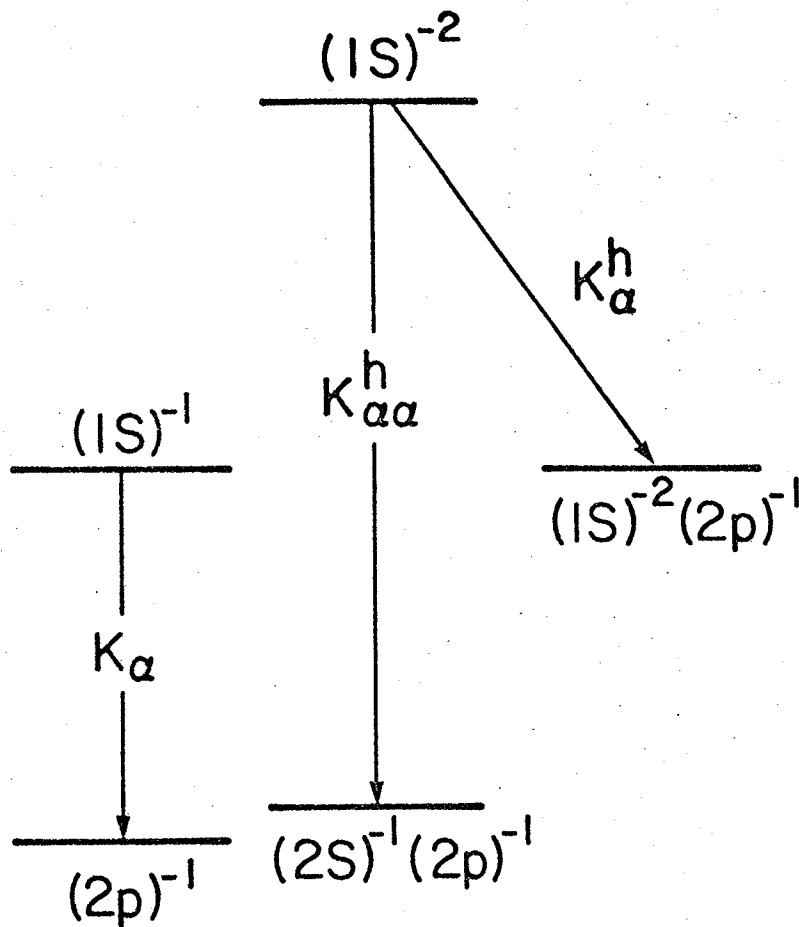


Figure 2.2 Energy level diagram showing the decay of doubly-ionized K-shell by the  $K_{\alpha}^h$  (hypersatellite) transition and  $K_{\alpha\alpha}^h$  (two-electron single-photon) transition. The normal ( $K_{\alpha}$ ) x-ray transition is also shown. (After Åberg et al., 1976)

equations (2.1) and (2.4) if the dependence of  $P_K$  on  $b$  is properly accounted for.

In table (2.1) predictions are presented for copper, rubidium and silver. The  $(K_{\alpha\alpha}^h/K_{\alpha})$  ratio was calculated by substituting into equation (2.1) values of  $P_K(b)$  from Hansteen et al. (1975) [labelled (1) in table (2.1)] and from equation (2.3) using the approximation of Kessel as suggested by McGuire and Richard (1973) [labelled (2) in table (2.1)]. The results in column (2) are approximately a factor of two higher than those in column (1). This discrepancy suggests that the approximation used in equation (2.2) is not strictly valid. The experiment described below will help to clarify the situation.

It is appropriate to point out that the x-ray cross-sections  $(\sigma_{1K})$  used in the calculation of  $(K_{\alpha\alpha}^h/K_{\alpha})$  ratios are those of Ramsay et al. (1978). These are found to be in excellent agreement with equation (5) of McGuire and Richard (1973) with  $G(V)$  values as given by Gerjuoy, Vriens and Garcia (McGuire and Richard, 1973).

The last column of table (2.1) is the energy of a proton which has the same velocity as the orbital K electrons in the elements considered. The relevance of this particular energy is discussed further below.

### 2.2.3 Criteria for the Experiment:

It is clear from the preceding treatment and the information given in table (2.1) that an experimental test of multiple ionization theory will have to satisfy several stringent requirements. First of all the projectile has to be a fully stripped ion of mass much greater than

Table 2.1 Theoretical predictions of single photon to normal  $K_{\alpha}$  intensity ratio ( $K_{\alpha\alpha}^h/K_{\alpha}$ ), single photon energy ( $E_{K_{\alpha\alpha}^h}$ ) and optimum energy of the bombarding proton for copper, rubidium and silver.

| Element  | Atomic Number | $(K_{\alpha\alpha}^h/K_{\alpha})$ Ratio |                      | $E_{K_{\alpha\alpha}^h}$ (KeV) | Bombarding Proton Energy $E_p$ (MeV) |
|----------|---------------|---|----------------------|--------------------------------|--------------------------------------|
|          |               | (1)*                                    | (2)†                 |                                |                                      |
| Copper   | 29            | $1.9 \times 10^{-7}$                    | $4.4 \times 10^{-7}$ | 16.278                         | 17                                   |
| Rubidium | 37            | $6.3 \times 10^{-8}$                    | $1.5 \times 10^{-7}$ | 26.963                         | 28                                   |
| Silver   | 47            | $2.3 \times 10^{-8}$                    | $5.4 \times 10^{-8}$ | 44.623                         | 47                                   |

\*  $(\sigma_{2K}/\sigma_{1K})$  calculated from Eq. (2.1) with  $P_K$  (b) values as given by Hansteen et al. (1975).

†  $(\sigma_{2K}/\sigma_{1K})$  calculated from Eq. (2.3) in the text.

the mass of the electron in order to obtain an accurate value for  $\sigma_{1K}$  (Garcia et al., 1968). This clearly favours the proton as a projectile. Furthermore, a proton velocity equal to that of the K-orbital electron of the target atom will enable an accurate value for R to be used in equation (2.3). It also has the advantage of giving the highest K x-ray yield.

As far as the target atom is concerned, it is obvious that an element exhibiting a high ( $K_{\alpha\alpha}^h/K_{\alpha}^h$ ) ratio is favoured. Of the elements given in table (2.1) copper satisfies this requirement. However, an independent experimental test\* shows that  $\gamma$ -rays from (p,n) reactions can cause considerable background in the region from 10 to 20 keV. The system described in section (2.3) was also not sensitive enough for another candidate, silver, to be used as a target. Therefore rubidium was chosen. Moreover, the Rb  $K_{\alpha}$  x-rays and the energy of its  $K_{\alpha\alpha}^h$  transition fall in the energy range where germanium detectors have very high efficiency and good resolution. The remaining part of this chapter therefore deals with the experimental aspects of this investigation.

---

\* Preliminary experimental test carried out by this author.

## 2.3 EXPERIMENT

### 2.3.1 Apparatus:

The single-photon experiments were carried out at the University of Manitoba Cyclotron Laboratory. The apparatus used for these experiments was normally used for proton induced x-ray emission (P.I.X.E.) studies. The technique is discussed in detail elsewhere (McKee et al., 1981, Lapointe, 1981). It incorporates a beam cube of side 20.32 cm (8") as the scattering chamber and a target holder, with a high resolution hyper-pure germanium detector (HPGe) as the x-ray counter. The HPGe sits at  $90^\circ$  to the direction of the beam. The face plate of the cube has a window of  $50.8 \mu\text{m}$  (0.002") Kapton allowing detection of x-rays at  $90^\circ$  with respect to the proton beam. The target is mounted on a target ladder which is introduced vertically through the top of the cube. The normal to the target may be oriented at angles between  $35^\circ$  and approximately  $55^\circ$  with respect to the proton beam.

For the present investigation the apparatus was set up as shown in figure (2.3). The target rotation was  $45^\circ$ . For these runs aluminium absorbers of various thicknesses were placed between the target and detector to cut down the  $K_\alpha$  x-ray flux and thus reduce pile-up in the electronics. In some of the runs, it was found useful to add a paraffin block 20 mm in thickness between the target and the aluminium absorber. This acted as a "proton stopper" to stop protons that scatter off the target from hitting the kapton window and Al absorber which would have excited x-rays from these materials and given rise to measurable background. The case for using aluminium as an absorber will be

presented in a later subsection.

### 2.3.2. The Rubidium Target:

Several targets were made by evaporating RbCl salt onto a thin mylar foil. The target holder subtended a small angle (approximately  $5^\circ$ ) at the boat, where the RbCl salt was placed. This meant that the variation in thickness across the target was of the order of 1%. The targets used in the experiments reported here had thicknesses of  $11.8 \text{ mg/cm}^2$  and  $9.1 \text{ mg/cm}^2$  of RbCl. The thickness was known to an accuracy of 1%. The thicknesses of the mylar backings used were  $9 \text{ }\mu\text{m}$  and  $4 \text{ }\mu\text{m}$  respectively. A thin ( $\sim 10 \text{ }\mu\text{g/cm}^2$ ) layer of high purity copper was deposited on the RbCl target in order to prevent flaking of the target material. It also served to make the target surface conducting thus reducing bremsstrahlung background which would have resulted from charge build-up on the target. Since RbCl is hygroscopic, targets were stored in an evacuated dessicator after preparation.

### 2.3.3. The Absorber:

The absorber has to be chosen such that, while drastically attenuating the Rb  $K_\alpha$  x-rays, the transmission in the region of the single-photon energy is kept at a reasonable level. If the latter is  $t$  and the ratio of the transmission at the single-photon energy to the transmission of the  $K_\alpha$  x-ray is  $r$ , then  $r$  and  $t$  are simply related by the formula:

$$r = \exp \left[ - \left( \frac{\mu_\alpha - \mu_{\alpha\alpha}}{\mu_{\alpha\alpha}} \right) \ln t \right] \quad \dots (2.8)$$

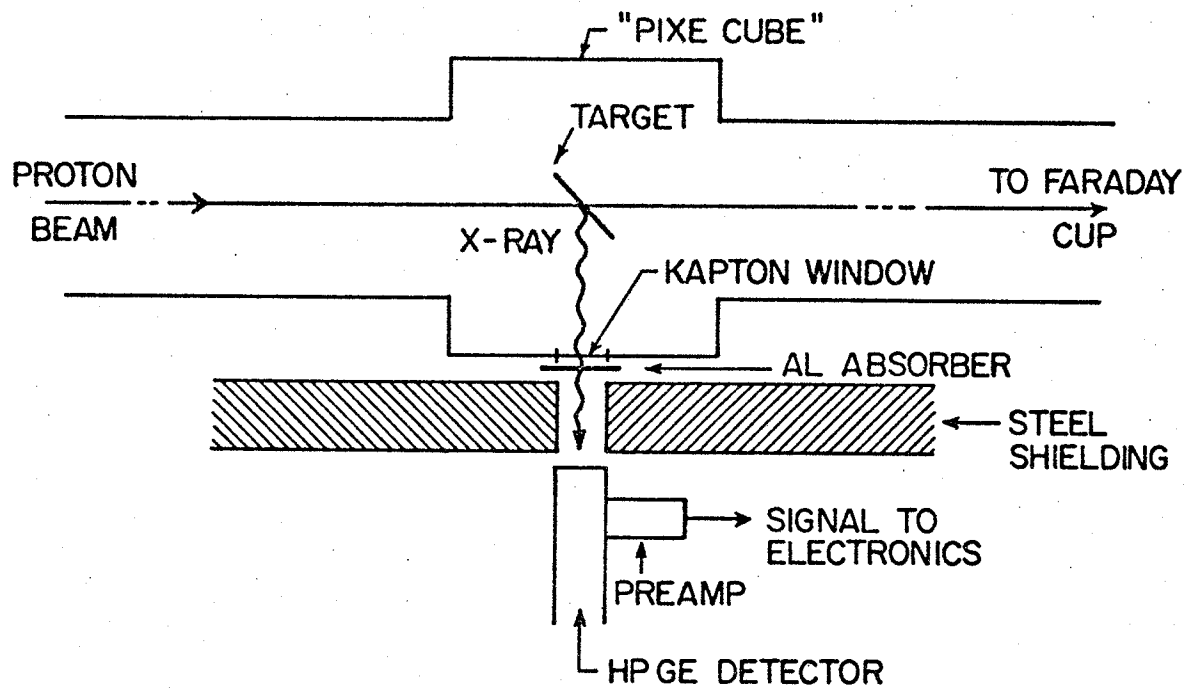


Figure 2.3 Diagram of the experimental setup used for two-electron single-photon studies.

where  $\mu_{\alpha}$  and  $\mu_{\alpha\alpha}$  are the mass attenuation coefficients of the absorber material at the Rb  $K_{\alpha}$  and  $K_{\alpha\alpha}^h$  energies respectively. Clearly the larger  $r$  is for a given  $t$ , the more effective is the absorber. Since  $\ln t$  is negative,  $r$  is maximized by choosing a material with the highest possible value for  $(\mu_{\alpha} - \mu_{\alpha\alpha})/\mu_{\alpha\alpha}$ . Furthermore the absorber material has to be available in a pure form and be reasonably easily made into the form of a disc.

In table (2.2) values of  $(\mu_{\alpha} - \mu_{\alpha\alpha})/\mu_{\alpha\alpha}$  are presented for materials that have been considered as candidates. The mass attenuation coefficients of Veigle (1973) have been used in this calculation. On this count alone aluminium is the first choice. Furthermore, its availability in the form of a highly pure (>99%) foil makes it possible to make absorbers of various thicknesses rather easily.

#### 2.3.4. The HPGe Detector:

The detector used for these experiments was an Ortec model 1113-10205 HPGe low energy photon spectrometer (Ortec Nuclear Catalogue, 1976). It has an active depth of 7 mm and an active area of 78.5 mm<sup>2</sup>. The resolution was measured with an IAEA <sup>57</sup>Co source and was found to be 230 eV FWHM at 14.4 keV.

A quantity  $\epsilon$  that enters into the calculation of single photon results (see § 2.4.4.) relates the detection efficiency for Rb  $K_{\alpha}$  x-rays to the detection efficiency at the single-photon energy. This factor written explicitly is:

$$\epsilon = \frac{\eta ( \text{Rb } K_{\alpha} )}{\eta ( \text{Rb } K_{\alpha\alpha}^h )} \quad \dots(2.9)$$

Table 2.2 Parameters relating to the choice of the absorber material.

| Material         | Atomic Weight<br>(gm per mole) | $\frac{\mu_{\alpha} - \mu_{\alpha\alpha}}{\mu_{\alpha\alpha}}$ | Order of<br>Preference |
|------------------|--------------------------------|--|------------------------|
| Aluminium        | 26.98                          | 6.76   | 1                      |
| Iron             | 55.85                          | 6.08   | 2                      |
| Sodium<br>Iodide | 149.89                         | 5.51   | 3                      |

Equation (2.9) suggests that a knowledge of  $\eta$  as a function of energy is necessary. Since  $\epsilon$  is a ratio, it is sufficient to determine the relative efficiency of the detector ( $\eta_r$ ) as a function of energy. This argument is clarified further below. The PIXE technique has been used to determine  $\eta_r(E)$  in the energy range  $8 \text{ keV} < E < 80 \text{ keV}$ .  $\epsilon$  can then be calculated by direct application of equation (2.9) above. The procedure was as follows:

Targets of copper, rubidium, rhenium, gold and bismuth were fabricated with known amounts of the element involved. Each of these targets contained a known amount of dysprosium which served as an internal standard. The detection efficiency of the Dy  $K_{\alpha}$  x-rays (45.6 keV) is taken to be 100%. These targets were bombarded, in turn, with a beam of 30 MeV protons in a normal PIXE experiment. The procedure is documented in detail elsewhere (Ramsay et al., 1978 and Lapointe, 1981). The relative efficiency  $\eta_r(E)$  is given by:

$$\eta_r(E) = \frac{\eta(E)}{\eta(45.6 \text{ keV})} = \frac{C_E}{C_{Dy}} \cdot \frac{N_E}{N(\text{Dy } K_{\alpha})} \quad \dots(2.10)$$

where  $N_E$  is the number of x-ray events at an energy  $E$  and  $N(\text{Dy } K_{\alpha})$  is the number of Dy  $K_{\alpha}$  x-rays. The constants  $C_E$  and  $C_{Dy}$  may be calculated from a knowledge of x-ray cross-sections, fluorescence yields, ...etc. (e.g. Ramsay et al., 1978). In this fashion  $\eta_r(E)$  was obtained in the energy range 8 keV to 80 keV. From these results  $\epsilon$  was found to be  $(0.60 \pm .01)$ .

### 2.3.5. Electronics:

The electronic circuit used is shown in figure (2.4). X-ray events

from the HPGe, which has its own built-in preamplifier, were transferred to the cyclotron control room to an ORTEC 572 spectroscopy amplifier. This has a pile-up rejection capability. This feature of the ORTEC 572 spectroscopy amplifier was particularly useful in dealing with possible detection of two K $\alpha$  x-rays which would interfere with the detection of single photon events. If signals corresponding to two events were detected within 6 $\mu$ s, but no less than 100 ns, of each other, the pile-up gate was closed and neither signal was passed on to the ADC. Signals less than 100 ns apart were not resolved and were treated as a single signal by the pile-up gate. Events passing the pile-up test were routed to an ADC, labelled in figure (2.4) as ADCO.

For the purpose of continuously monitoring the performance of the pile-up rejection circuit, the raw x-ray events from the amplifier were routed through a second ADC to a different region in the data file (marked "HPGe ungated" in figure 2.4). A comparison of the two regions enabled an immediate test of the pile-up rejection circuit to be made. The ratio of pile-up events to the expected number of single-photon events was less than 0.01 in all the runs. For example, in the third single-photon run described in §2.4.3, the number of pile-up events per day was 5. This is to be compared with an expected rate of single-photon events of 600 events per day. These figures were calculated according to equation (2.1) of Birchall et al. (1978). The circuit used here was subjected to tests recommended by these authors and its performance was found to be satisfactory for the present purpose.

Energy spectra were collected on-line with the data acquisition program MIRAD. The data were taken in 1024-channel binary files and stored on DEC tape for later analysis on a PDP15/40 computer.

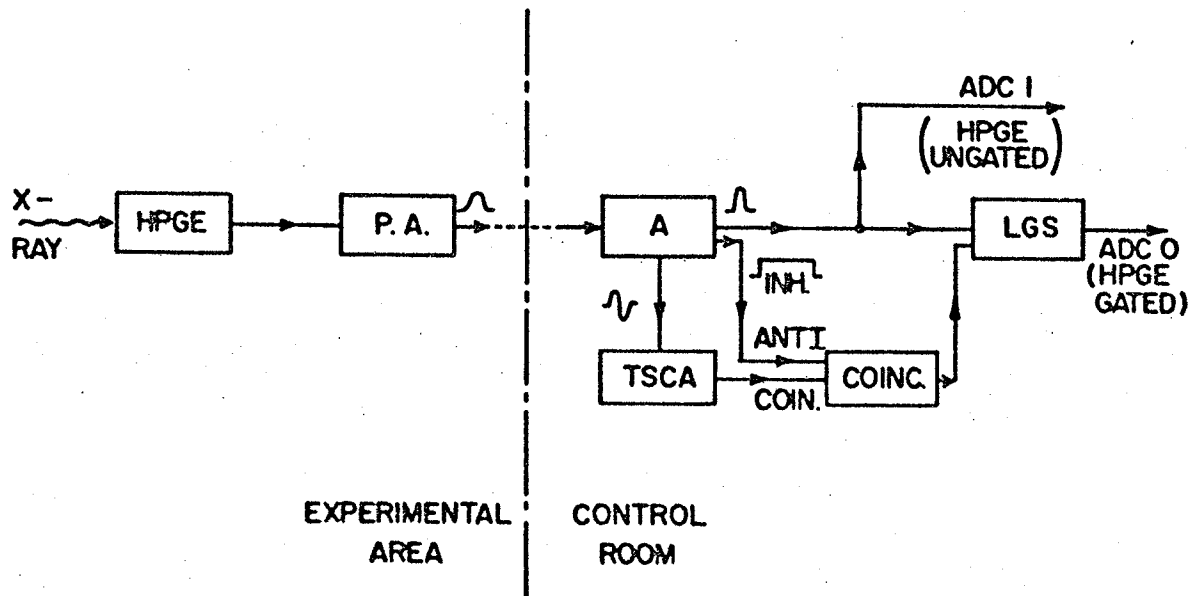


Figure 2.4 Electronics diagram: P.A.: pre-amplifier, A: ORTEC 572 spectroscopy amplifier with built-in pile-up rejection capability, TSCA: timing single channel analyser, COINC: coincidence unit, LGS: linear gate and stretcher, ADC: analogue-to-digital converter.

## 2.4. EXPERIMENTAL PROCEDURE

### 2.4.1. Spectrum Calibration:

The energy spectra were calibrated before, during and after the runs using an  $^{241}\text{Am}$  source. A linear least square fit to the calibration data indicated no significant deviation from linearity. The energy scale was 40 eV per channel. A continuous monitoring of gain fluctuations is provided by the position of the Rb  $K_{\alpha}$  and  $K_{\beta}$  x-rays. They remained constant throughout the experiment to within  $\pm 0.5$  channel ( $\pm 20$  eV) and thus served as an additional check on the calibration.

### 2.4.2. Beam Monitoring:

It was not necessary to monitor the proton beam accurately since the aim of the experiment was the measurement of the single-photon transition rate relative to the x-ray emission rate. However, a knowledge of the beam current incident on target was required in order to determine the transmission of the Rb  $K_{\alpha}$  and  $K_{\beta}$  x-rays in the absorbers employed in these runs (see § 2.4.4). These data were used to calculate the transmission of the single-photon line. For this purpose the proton beam was monitored using a suppressed Faraday cup whose output was fed into a current integrator and then to a scaler.

Faraday cup readings were also used to verify that the observed  $K_{\alpha}$  cross-section was in agreement with values measured previously (Ramsay et al., 1978). Furthermore, the constancy of the x-ray yield per unit charge throughout these experiments indicated that there was

no loss of target material and therefore no target deterioration caused by radiation. The latter would have made it difficult to take into account self-absorption of  $K_{\alpha}$  x-rays and single-photon events in the target material in a proper fashion.

### 2.4.3. Single-Photon Search:

Three separate runs were carried out in an attempt to measure the ( $K_{\alpha\alpha}^h/K_{\alpha}$ ) ratio for rubidium. These runs were basically similar but differ in detail. They will be discussed in the order in which they were performed.

In the first run, a current of approximately 11 nA of 28 MeV protons was used to bombard the  $9.1 \text{ mg/cm}^2$  thick target of RbCl. At this energy the K x-ray yield, and presumably the probability of single photon events is at a maximum. An aluminium absorber 3.6 mm in thickness was placed 10 cm from the target and just outside the kapton window. The HPGe was placed 13.2 cm from the kapton window. This run lasted for 91.8 hours.

The second run used a thicker RbCl target ( $11.8 \text{ mg/cm}^2$ ) and Al absorber (4.7 mm). The detector to kapton window distance was reduced to 3.6 cm and the beam current to 3.5 nA. The duration of this run was 20.6 hours.

In the third run the beam current was increased to 50 nA and a 3.4 mm Al absorber and a 20 mm paraffin proton stopper were used. In order to limit the count rate in the electronics to a desirable level, the upper and lower thresholds of the single channel analyser were

adjusted such that only x-ray events in the energy range of interest were recorded. This run lasted for 257.6 hours and the resulting spectrum is shown in figure (2.5). The data are scaled by a factor of 1/40. The shape of the background may be explained by considering the transmission of photons in matter as a function of energy (Price et al., 1957).

Peaks in figure (2.5) that do not correspond to the target material are believed to arise from impurities in the Al absorber. This applies to cadmium, silver and tin. The peak near channel 850 is due to tantalum. This contaminates the target since the RbCl material is evaporated using a tantalum boat. The apparently large size of the Ta peak is due to the fact that its energy is in a region where the absorber is ineffective.

#### 2.4.4. Data Analysis:

It is clear from figure (2.5) that no peak corresponding to the  $K_{\alpha\alpha}^h$  energy was observed in any of the runs. The data analysis was aimed, therefore, at establishing an upper limit on the  $(K_{\alpha\alpha}^h/K_{\alpha})$  ratio.

The upper limit, with 95% confidence, for the number of counts in a peak sitting on a background several orders of magnitude larger in size corresponds to twice the square root of the number of background counts in the area lying under the peak. The single photon peak is assumed to be 11 channels wide ( $\approx 440$  eV). This assumption is consistent with the measured resolution of the HPGe detector. It is relevant to note that the FWHM of the 26.35 keV  $\gamma$ -ray from  $^{241}\text{Am}$  as measured by the

Figure 2.5 Single-photon energy spectrum: pile-up rejection circuit,  $11.8 \text{ mg/cm}^2$  RbCl target, 3.4 mm Al absorber plus 20 mm paraffin proton-stopper. The spectrum is scaled by a factor of  $1/40$ . The region in which the single-photon peak is expected to appear is shown in an expanded form.

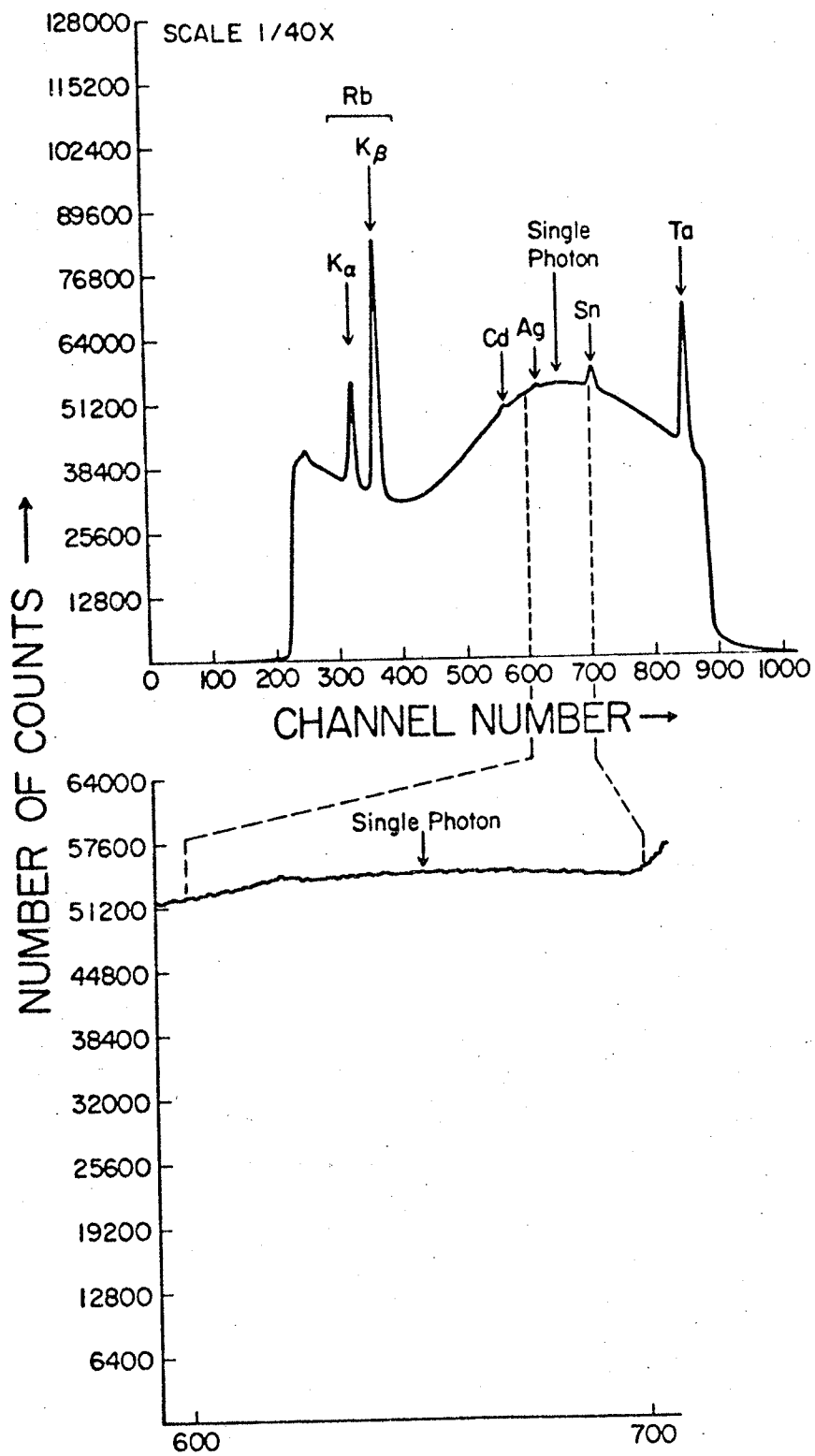


Figure 2.5

HPGe detector was 11 channels. In this case the upper limit on the ratio observed in a particular run would be:

$$(K_{\alpha\alpha}^h/K_{\alpha}) < [2\sqrt{N_b}/N_{K_{\alpha}}] a.\epsilon \quad \dots(2.11)$$

where  $N_b$  is the number of background counts observed and  $N_{K_{\alpha}}$  is the number of  $K_{\alpha}$  events recorded. "a" is the factor expressing the transmission of  $K_{\alpha}$  x-rays in comparison with expected single-photon events in the kapton window, absorbers and air path. It is related to r of equation (2.8). Its determination is discussed in detail below.  $\epsilon$  is a factor accounting for changes in the efficiency of the HPGe detector with photon energy as defined in equation (2.9). Its value has already been determined in §2.3.4. The upper limit with 67% confidence level is half of that given by equation (2.11) above.

This method of analysis has been shown to give results which are in very good agreement with predictions based on the Poisson distribution (Birchall et al., 1978).

The factor expressing the relative transmission was obtained by measuring the transmission directly. In the case of Al absorbers and paraffin proton stopper the transmission was measured using the K x-ray line from the target itself on runs with and without absorbers in place. These measurements were checked using an  $^{241}\text{Am}$  source and reasonable agreement was obtained. The error in the measurement of the transmission through the Al absorbers was 8% for the 3.6 mm and 3.4 mm absorbers and 5% for the 4.7 mm absorber. The error in the measurement of transmission through the paraffin block used in the third single-photon run amounted to 6.4%. These errors in measurement form the sources of uncertainty in the transmission factor "a" defined earlier

and are shown as an error in "a" in table (2.3). They amount to 3.6% for the first single-photon run, 8.7% for the second run and 11% for the third run.

Transmission measurements were then corrected for attenuation in the kapton window, air path and the Be window of the detector. The correction is 0.8% for 50.6  $\mu\text{m}$  kapton, 5.1% for 13.2 cm air path (kapton window to detector distance in the first run), 3% for 3.6 cm air path (Kapton window to detector distance in the second and third runs) and 0.6% for the 127  $\mu\text{m}$  Be window. These corrections were calculated using the mass attenuation coefficients of Veigle (1973). The corrections amount to 6.5% for the first single-photon run and 4.4% for the second and third runs.

A further correction factor due to self-absorption in the target was also included. This correction takes into account the fact that the x-ray events originate from the entire bulk of the target and not only the surface. First of all, it was necessary to determine whether or not the attenuation of the Rb x-rays in the RbCl target was linear for the target thicknesses of interest (up to a maximum of 11.8  $\text{mg}/\text{cm}^2$ ). In order to do that, RbCl targets of various thicknesses (0.58  $\text{mg}/\text{cm}^2$  to 11.8  $\text{mg}/\text{cm}^2$ ) were fabricated by the evaporation process outlined in §2.3.2. and then irradiated with a beam of 28 MeV protons in a typical PIXE experiment (McKee et al., 1981). The results of this test indicated that the number of Rb K x-rays per unit charge per unit thickness of RbCl was constant over the range of thicknesses investigated (0.58  $\text{mg}/\text{cm}^2$  to 11.8  $\text{mg}/\text{cm}^2$ ). This meant that the attenuation of the x-rays in the target can be accounted for by simple integration over

the target thickness. The correction to the factor "a" due to self-absorption was found to be 3% for the 9.1 mg/cm<sup>2</sup> thick RbCl target while it was 4% for the 11.8 mg/cm<sup>2</sup> thick RbCl target. The mass attenuation coefficients of Veigle (1973) were used in order to obtain these results.



## 2.5 RESULTS AND CONCLUSIONS

The results of the analysis of the data from the various runs are shown in table (2.3). The data are presented in the form of an upper limit on the ratio of two-electron single-photon to one-electron single-photon transitions, i.e.  $(K_{\alpha\alpha}^h/K_{\alpha})$ , at 95% and 67% confidence levels. Tabulated along with these results is the best result available prior to this work. The limit was obtained using a 3.4 mm Al absorber and a 20 mm paraffin block as a proton-stopper. The required level of sensitivity of less than  $10^{-7}$  has been achieved. The present measurement suggests that the theoretical models outlined in §2.2 may not describe the transition process successfully. Therefore the numerical predictions, based on calculations employing these models and listed in table (2.1), may overestimate the magnitude of the  $(K_{\alpha\alpha}^h/K_{\alpha})$  ratio. The existing theory, then, may include assumptions that do not account for the correlated transition process correctly. It is also demonstrated that the "prescription" for calculating multiple ionization cross-sections suggested by McGuire and Richard (1973) gives results which are in excess of two times higher than the predictions of the impact parameter model.

CHAPTER THREE

DESIGN AND FEASIBILITY STUDY

OF A PROTON MICROPROBE FOR

K X-RAY STUDIES

### 3.1 THE ROLE OF K X-RAYS AS AN ANALYTICAL TOOL

By way of an introduction to this chapter, the value of x-rays as an analytical tool is briefly discussed. Special emphasis is placed on the study of K x-rays induced by 20-50 MeV protons, an activity which has been in progress at the University of Manitoba Cyclotron Laboratory for the past eight years.

Particle induced x-ray emission (P.I.X.E.) has become a widely used tool in the microanalysis of biological, environmental and metallurgical samples. Detailed accounts of the technique can be found elsewhere in the literature (Johansson et al., 1972, Garcia et al., 1973, Deconninck et al., 1975). PIXE is a powerful tool for a variety of reasons: It is non-destructive and has a high sensitivity in terms of p.p.m. and even p.p.b. due to the development of high resolution x-ray detectors. Inherent difficulties with the technique are: The requirement of an accurate knowledge of x-ray production cross sections as a function of incident particle energy for all elements under consideration, and at low energies, difficulty in unfolding peaks in the observed spectra.

Most laboratories interested in PIXE work use proton beams of 1-5 MeV in energy from Van de Graaff accelerators. This is due more to the relative abundance of such accelerators than to any suggestion that their energy range is the optimum for x-ray studies. Furthermore, there has been a widely-held belief that Compton scattering at higher energies would produce a high enough background to obscure the x-rays (Gérve and Schatz, 1975). This is however not the case and the situation is clarified below.

Much clean P.I.X.E. work has been done at the University of Manitoba Cyclotron Laboratory using protons in the 20-50 MeV energy range. Two main objectives are identified with this work: i) An understanding of the process of K-shell ionization and of x-ray emission following it. ii) The use of K x-ray fluorescence as a tool in microanalysis. The first objective is of interest mainly because of the fundamental physics involved, however, it is largely motivated by the second. The usefulness of K x-rays induced by 20-50 MeV protons as an analytical tool is summarized as follows:

a) K x-ray yields are maximal for medium Z elements with 20-50 MeV protons (Ramsay et al., 1978).

b) The technique yields high quality information with low underlying background (Wilk et al., 1977).

c) Simultaneous analysis of a sample for all elements above Z=10 is possible.

d) K x-rays from adjacent elements in the periodic table are well separated and are easily resolved by a suitable germanium detector.

e) K x-rays are much less attenuated by thin targets than L x-rays. For typical targets self-absorption is negligible for K x-rays, whereas for L x-rays it may be significant. For example, a gold target thin enough to transmit 95% of gold K x-rays will only transmit 10% of the L x-rays.

f) proton energy loss in the target can be small. This is especially true for targets that have been used so far (typical thickness of  $\approx 500 \mu\text{g}/\text{cm}^2$ ).

g) accurate measurement of K x-rays emitted as a result of proton bombardment may be performed using intrinsic germanium detectors which

have excellent energy resolution (for example 230 eV at 14.4 keV and 448 eV at 122 keV) and high efficiency.

So far only bulk samples have been investigated. Particular projects have concerned the study of possible biohazards of cesium ions (Pinsky 1981) and an investigation of the correlation between trace element contents in hair and mental retardation in children (Balasko and Brockman, 1981).

The next step in the development of a precise tool for trace element determination would be to establish a device which is capable of focusing an incident proton beam to a diameter of the order of 10  $\mu\text{m}$ . A beam of this size can then be scanned across a sample to obtain positional information on the distribution of elements within the sample and to establish physical form. Such a beam would be used in microstructure studies and in the investigation of health hazards in the environment. Applications of the facility are briefly discussed in a later section of this chapter. The focusing system required is commonly referred to as a proton microprobe. It can be thought of as a scanning proton microscope. The purpose of this chapter is to examine the feasibility of establishing such a system at the Cyclotron Laboratory of the University of Manitoba. The design considerations are discussed in the following section.

### 3.2 DESIGN CONSIDERATIONS

The proton beam leaves the cyclotron through a slit of dimensions 5 mm x 12 mm in x- and y-coordinates respectively and propagates along the z-axis. It is then focused by a quadrupole doublet (QD1,2) to produce a 4 mm x 4 mm spot 5.75 m further downstream (Figure 3.1). The field strengths required are presented in columns 3 and 4 of table (3.1). Each quadrupole has a half aperture of 52.7 mm and an effective length of 31.1 cm. The first quadrupole defocuses the beam in the x-z plane and focuses it in the y-z plane. The second quadrupole focuses the beam in the x-z plane and defocuses it in the y-z plane. The combined effect of the doublet is to produce a beam spot of the dimensions quoted above. The doublet is a general laboratory item used on beamlines for beam focusing. Beam spots of millimetre dimensions are readily obtainable in a standard beam-optics setting procedure. The function of the microprobe described below is to focus this beam down to micrometre dimensions.

At point C, where the beam is 4 mm in diameter, a system of collimators with diameters ranging from 20-70  $\mu\text{m}$  is placed (Figure 3.1). These allow a very small fraction of the beam to continue upon its journey to the target. The design is based on a 70  $\mu\text{m}$  diameter collimator. However, the argument applies to the full range of collimator diameters considered, as will become clear later on.

A system of four quadrupoles is placed 3.5 m further downstream from the collimator slit C (Figure 3.2). This set of quadrupoles focuses the beam down to 10  $\mu\text{m}$  diameter. It is commonly known as the "Russian

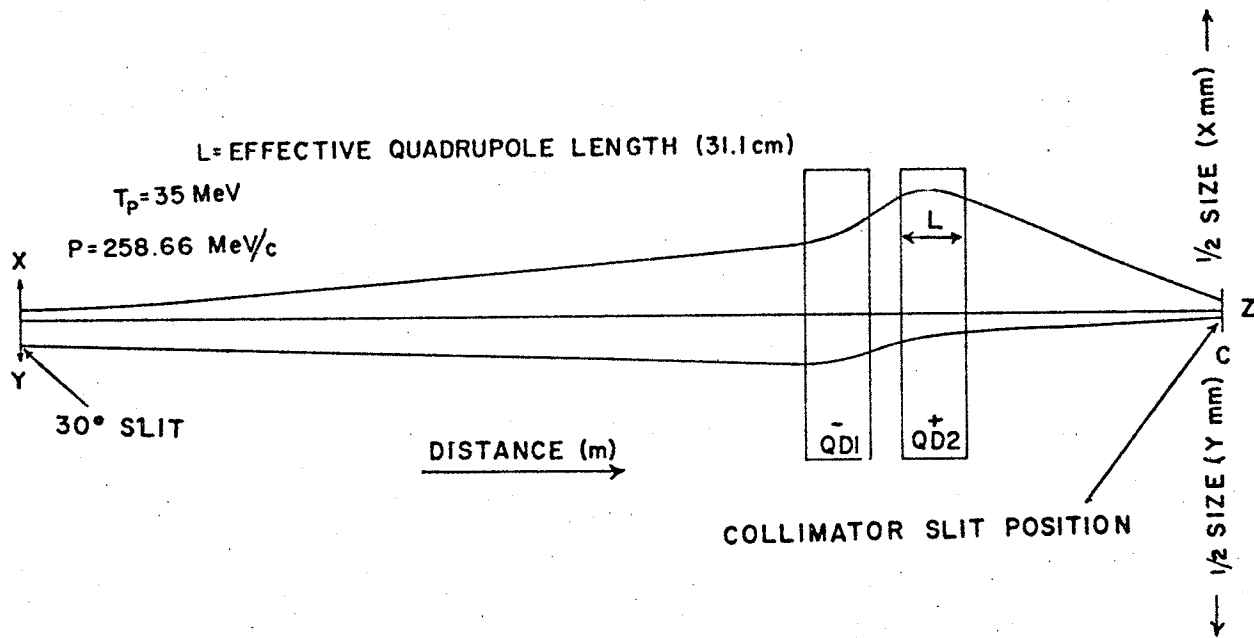


Figure 3.1 Focusing the proton beam from the cyclotron to millimetre dimensions using a quadrupole doublet (QD1,2).

quadruplet". The first order properties of the system have been studied by Dymnikov et al. (1965). This lens configuration has been one of the most popular and most successful in low energy (few MeV) microprobes (e.g. Cookson and Pilling 1973 and Cookson et al., 1972). This is because of its symmetry and its orthomorphic character (Legge 1982). This means that the magnetic fields can be arranged in such a way that aberrations are cancelled or at least minimized.

Each of the four quadrupoles has an aperture diameter, pole tip to pole tip, of 5.4 cm and is 18.05 cm in length (21.15 cm effective length). Neighbouring quadrupoles are separated by 4.5 cm. The first and fourth quadrupoles (outer doublet) have equal but opposite fields, as have the second and third quadrupoles (inner doublet). The inner doublet is oriented at  $90^\circ$  relative to the outer doublet. The field strengths as a function of proton energy for the system of quadrupoles comprising the microprobe are tabulated in columns 5 and 6 of table (3.1). Field stability is a very important factor, as is the relative orientation of the quadrupoles. Imperfect alignment can introduce serious twist problems which will throw the beam out of focus (Kneis et al., 1982). This and other design aspects will be discussed later on in this section.

A system such as that described above will focus a 35 MeV proton beam emerging from a collimator slit of 70  $\mu\text{m}$  diameter to a spot of 10  $\mu\text{m}$  diameter at a distance of 3.1 cm from the exit of the fourth element of the quadruplet system of magnets. The demagnification of 1/7 is expected to be smaller for particle energies less than 35 MeV and for collimator diameters smaller than 70  $\mu\text{m}$ . The reasons for this are that the lower the proton energy, the less the field strength

Table 3.1 Quadrupole field strengths as a function of beam energy.

| $T_p$ (MeV) | $P$ (MeV/c) | $-Q_{D1}$<br>(mT) | $Q_{D2}$<br>(mT) | $\pm Q_0$<br>(mT) | $\pm Q_I$<br>(mT) |
|-------------|-------------|-------------------|------------------|-------------------|-------------------|
| 20          | 194.76      | 156.23            | 197.29           | 252.14            | 545.78            |
| 25          | 218.03      | 174.90            | 220.86           | 282.27            | 610.99            |
| 30          | 239.16      | 192.03            | 242.34           | 309.62            | 670.21            |
| 35          | 258.66      | 207.69            | 262.10           | 334.87            | 724.85            |
| 40          | 276.88      | 222.10            | 280.47           | 358.46            | 775.91            |
| 45          | 294.06      | 236.12            | 297.97           | 380.70            | 824.05            |
| 50          | 310.37      | 249.09            | 314.12           | 401.81            | 869.76            |

$T_p \equiv$  proton energy (MeV)

$P \equiv$  proton momentum (MeV/c)

Focuses the beam to 4 mm diameter

$Q_{D1} \equiv$  field strength of the "first quad" used to focus the beam on the collimator slit (-ve; defocuses in x, focuses in y)

$Q_{D2} \equiv$  field strength of the "2nd quad" used to focus the beam on the collimator slit (+ve; focuses in x, defocuses in y)

Focuses the beam to 10  $\mu$ m diameter

$Q_0 \equiv$  field of the first and fourth (outer) quadrupoles of the quadruplet

$Q_I \equiv$  field of the second and third (inner) quadrupoles of the quadruplet

required to focus the beam; and the smaller the collimator slit diameter, the smaller the maximum diameter of the beam envelope will become.

The overall design is shown in figure (3.2), along with a calculated beam profile. Beam optics calculations have been performed with the program TRANSPORT (Brown 1972). The target position is marked. Beam currents as a function of collimator diameters are tabulated in table (3.2). This calculation is based on 1  $\mu\text{A}$  of beam current emerging from the cyclotron, a figure which is rather conservative. The current density produced at the target is approximately  $(3.8 \pm 0.4) \text{ pA} \cdot \mu\text{m}^{-2}$ . Beam parameters at important stages of propagation are tabulated in table (3.3). These, together with the data of tables (3.1) and (3.2) and figures (3.1) and (3.2) look promising.

Scanning of the sample with the microbeam may be achieved by mounting the target holder on a micrometer arrangement which can be freely moved in the x- and y- directions. This method is preferable to that of deflecting the beam with the aid of electrostatic steering. The latter causes a deterioration of the quality of the focal point of the beam spot as deflections away from the central axis are increased due to stray electric and magnetic fields.

Beam profile may be measured by scanning a fine wire across the beam and observing the characteristic x-rays emitted as a result of bombardment of the wire by the proton beam. This method has already been used successfully in conjunction with the study of slit scattering carried out in this laboratory and discussed further below. Another method is observing the width of radiation damage caused by the proton

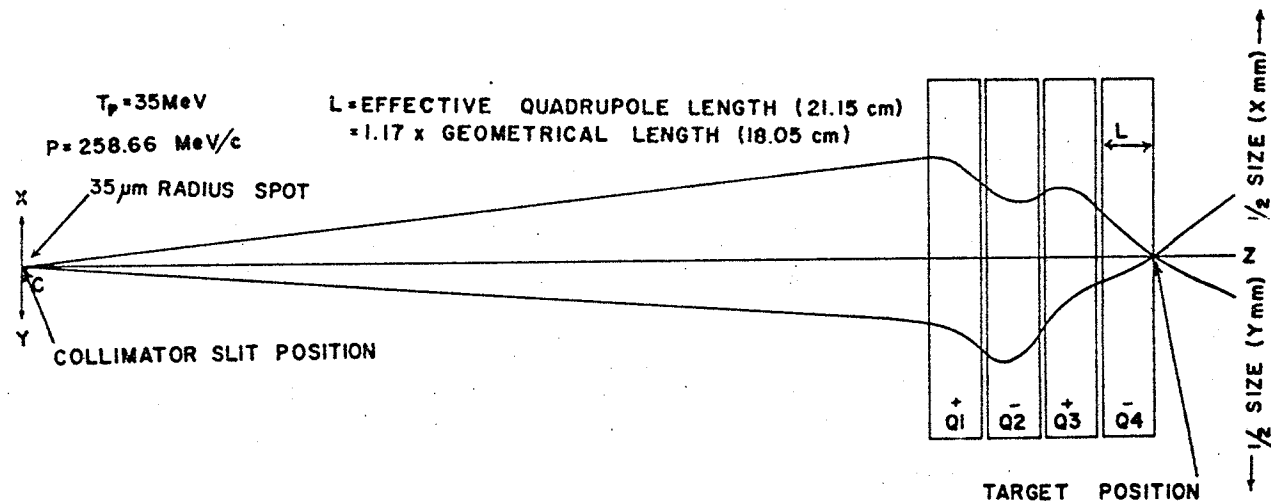


Figure 3.2 Layout of the proposed proton microprobe. A calculated beam profile in x- and y- planes is shown.

Table 3.2 Current on target as a function of collimator diameter.

| d( $\mu\text{m}$ ) | F                 | I <sub>T</sub> (pA) |
|--------------------|-------------------|---------------------|
| 20                 | $4.0 \times 10^4$ | 25                  |
| 30                 | $1.8 \times 10^4$ | 56                  |
| 40                 | $1.0 \times 10^4$ | 100                 |
| 50                 | $6.4 \times 10^3$ | 160                 |
| 60                 | $4.4 \times 10^3$ | 230                 |
| 70                 | $3.3 \times 10^3$ | 300                 |

d  $\equiv$  diameter of collimator slit ( $\mu\text{m}$ )

F  $\equiv$  factor by which beam current is reduced

I<sub>T</sub>  $\equiv$  current on target based on 1 $\mu\text{A}$  emanating from 30° slit and incident on the collimator slit

beam within a thin plastic scintillator foil. The method has been used by Heck (1978) and proved to be useful. In addition to these methods, there is the usual method of directly observing the beam with the aid of an optical microscope (Cookson and Pilling, 1973).

So far the overall design of the microprobe has been discussed in detail. In the remaining part of this section some of the practical problems that might be encountered are qualitatively discussed.

The first problem is that of slit scattering at the collimator C (figure 3.2). This topic has been examined in detail by Burge and Smith (1961) who conclude that the amount of slit scattering is roughly proportional to  $(A/\rho Z^{1/2})$ . A,  $\rho$  and Z are the atomic weight, density and atomic number of the slit material respectively. This favours elements such as nickel and tantalum. As a first step in the study of the relevance of slit scattering to the present microprobe design four types of slits have been made out of stainless steel. These are depicted in figure (3.3). Slit type (a) was chosen because of its simple geometry. Slit type (d) has been suggested by Nobiling et al. (1975) who claim to have achieved a ratio of intensity in the beam spot to that in the halo of  $10^8$ . Slit types (b) and (c) were chosen because they are simpler to machine than slit type (d). Each slit was 1 mm wide and was placed in turn in the parallel proton beam. The emerging collimated beam was detected by scanning with an indium wire. The indium  $K_{\alpha}$  x-rays emitted, as a result of the indium wire intercepting the proton beam were then detected with a hyperpure germanium detector. The ratio of the number of  $K_{\alpha}$  x-rays detected to the number of incident protons enabled a determination of the divergence of the beam due to slit

Table 3.3 Beam parameters\*

| POSITION   | X          | $\theta_x$ | Y          | $\theta_y$ |
|--|------------|------------|------------|------------|
| 30° slit (waist in X but not in Y)   | 2.5 mm     | 4.5 mr     | 6.0 mm     | 1.21 mr    |
| emittance  | 35.3 mm.mr |            | 22.7 mm.mr |            |
| collimator slit (focus in X and Y) (70 $\mu$ m diameter collimator is placed at this position) | 2.02 mm    | 5.468 mr   | 2.0 mm     | 3.62 mr    |
| target position (waist)  | 5 $\mu$ m  | 40.472 mr  | 5 $\mu$ m  | 26.129 mr  |

\* X and Y represent the  $\frac{1}{2}$  size of the beam spot in X and Y directions.

$\theta_x$  and  $\theta_y$  represent the  $\frac{1}{2}$  angles of the beam in X and Y.

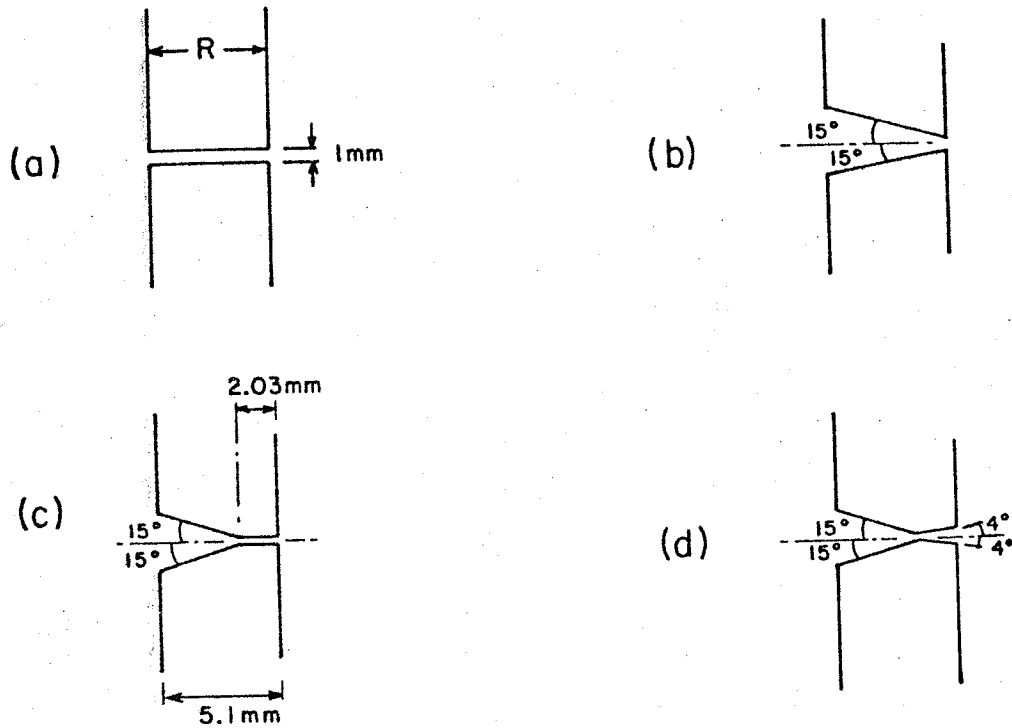


Figure 3.3 Types of slit designs investigated. (d) is the design proposed by Nobiling et al. (1975). R is equal to the range of the proton beam in steel.

scattering to be made. The FWHM of the resulting beam profile was typically 0.6 mm. This investigation was carried out at 35 MeV and 23 MeV. Preliminary results indicate that slit type (b) gives least divergence of the four types of slits examined (2% at 35 MeV). Slit scattering was approximately a factor of two higher at 23 MeV than at 35 MeV. These results are qualitative at this stage of the investigation and more work on this particular aspect of the design is necessary. It is suggested that 100  $\mu\text{m}$  wide slits are made and their properties are investigated systematically before a particular collimation scheme is chosen.

Scattering of protons from gas particles is not expected to be a problem for proton beams of 20-50 MeV as is the case for protons of a few MeV.

Minimising chromatic aberrations requires the spread in energy to be not more than 7 keV. This can be achieved by passing the beam through a  $45^\circ$  analysing magnet. A variation of the beam energy of this magnitude contributes less than 20% to the size of the beam spot at the target position.

Geometrical alignment problems behave linearly with field stability (Lobb, 1970). In this particular case the effects are less serious than those of chromatic aberrations since they are additive and may be eliminated by relative rotation of lens elements (Legge, 1982). Third order aberrations can be corrected by a suitably chosen octupole field at the quadrupole aperture (Heck, 1976).

### 3.3 APPLICATIONS

There are two excellent reviews which describe the applications of microprobes to various fields (Cookson 1979, Cahill 1980). Therefore it suffices here to discuss briefly several applications of special interest to research programs at the University of Manitoba.

Two particular areas will benefit greatly from the establishment of such a facility. The first is the study of the spatial distribution of cesium ions in tissue of mice injected with cesium. The interest here is in the environmental effects and toxicity of cesium (Pinsky 1981). The second area involves performing scans of individual strands of hair with the purpose of establishing the distribution of various trace elements in hair. The interest here is in the search for a correlation between trace element content in hair and Down's Syndrome (Balasko and Brockman, 1981). These two areas have already benefited from K x-rays as an analytical tool and bulk samples have already been analyzed using the PIXE technique. Preliminary results are promising.

Other areas of possible application are in the fields of materials science and earth science where trace element and particle size information are valuable assets.

### 3.4 CONCLUSIONS

In conclusion, it has been shown in this chapter that it is feasible in principle to construct a proton microprobe which focuses a 20-50 MeV beam of protons to micrometer dimensions. Preliminary results indicate that problems commonly encountered in the design and construction of such a facility are not insurmountable. However, the discussion presented in this chapter must be regarded as exploratory in nature at this stage and further work on the design details is necessary. This has already been pointed out at various points in the last section.

A note regarding the time scale involved in the construction of the microprobe is in order. Assuming the present capabilities of the mechanical and electrical workshops of the physics department of the University of Manitoba and that two graduate students<sup>\*</sup> work on the project as their theses topics, it should take approximately one year for the construction and test of the four lens elements comprising the microprobe and perhaps another year for the assembly of the device together with auxiliary equipment, e.g. suitable target holder, vacuum system, etc.

It is clear that the establishment of a microprobe facility at the University of Manitoba will further the progress of research in areas as diverse as environmental science, mental health (Down's Syndrome) and earth science.

Finally, it is appropriate to comment on how competitive such a

---

\*Messrs. A.R. Helaly and R. Prakash, two graduate students, have started working on the microprobe as their theses projects.

facility will be in comparison with microprobe facilities which exist or are planned elsewhere. Legge has recently surveyed proton and nuclear microprobe developments (Legge, 1982). In table 1 of Legge's article all microprobe facilities are shown with the most pertinent data on each. It is clear that all facilities, with the exception of the Hamburg microprobe, use particle beams of a few MeV energy for nuclear reaction, Rutherford Back Scattering (RBS) and PIXE studies. PIXE work in these laboratories utilizes K x-rays for light elements and L x-rays for heavy elements. Difficulties associated with this procedure have already been outlined in section (3.1) of this chapter. The Hamburg group (Brückmann et al., 1981) has reported on the successful completion of their microprobe facility which uses 10-30 MeV protons from the Hamburg cyclotron. They have achieved a spatial resolution of approximately 40  $\mu\text{m}$  and reported data on the spatial distribution of copper, strontium and calcium across samples. The Manitoba facility is designed to be an analytical tool, with better spatial resolution, for elements of higher Z values. This demonstrates its uniqueness.

APPENDIX A

CORRECTION FOR THE VECTOR POLARISATION

IN THE "m=0" STATE

The vector polarisation impurity in the m=0 state has already been discussed in subsection (1.3.5) of the text and is treated in detail by de Jong (1981). We start by the first of equations (1.19) and refer to it as equation (A.1) here:

$$p_z^0 = \frac{1}{2}(1 - \delta^+)(1 - \frac{1}{Q}) \quad \dots(A.1)$$

The left-right asymmetry  $\epsilon$  is given by (Ohlsen and Keaton, 1973):

$$\epsilon = \frac{3}{2} p_z A_y \quad \dots(A.2)$$

solving for  $\delta^+$  we obtain:

$$\delta^+ = 1 + \frac{4\epsilon/3A_y}{(1/Q - 1)} \quad \dots(A.3)$$

The deuteron analysing powers from  ${}^4\text{He}(\vec{d},d){}^4\text{He}$  of table (1.2) have been used to determine  $\delta^+$  values according to equation (A.3). The results as a function of proton laboratory angle are reported in table (A.1) and used to calculate the correct value of the tensor polarisation of the deuteron beam in equation (1.19) of the text.

Table A.1 Measured values of  $\delta^+$  at each angle.

| $\theta_p^{\text{lab}}$ ( $^\circ$ ) | $\delta^+$ |
|--------------------------------------|------------|
| 20                                   | -1.32      |
| 30                                   | 0.785      |
| 35                                   | 0.912      |
| 40                                   | 1.066      |

APPENDIX B

DEUTERON VECTOR AND TENSOR ANALYSING  
POWERS OF THE  ${}^4\text{He}(\vec{d},p){}^4\text{He}$  REACTION AT  
14.8 MeV INCIDENT DEUTERON ENERGY

In this appendix the data resulting from the experiment described in chapter one of the main text and presented in figures (1.6) and (1.7) are given in tabular form. The symbols used are self-explanatory and repeated here for convenience.  $E_p$  is the proton energy in MeV.  $A_y$  is the deuteron vector analysing power and the error associated with it  $\Delta A_y$ .  $A_{yy}$  is the deuteron tensor analysing power with its error  $\Delta A_{yy}$ .  $\theta_p^{\text{lab}}$  is the proton laboratory angle at which the measurement was carried out. The results are average values of left and right detector measurements except for the  $20^\circ$  data where results are those from the left detector only.

Table B.1:  $\theta_p^{\text{lab}} = 20^\circ$

| <u><math>E_p</math> (MeV)</u> | <u><math>A_y</math></u> | <u><math>\Delta A_y</math></u> | <u><math>A_{yy}</math></u> | <u><math>\Delta A_{yy}</math></u> |
|-------------------------------|-------------------------|--------------------------------|----------------------------|-----------------------------------|
| 4.136                         | 0.061                   | 0.062                          | -0.516                     | 0.206                             |
| 4.506                         | -0.020                  | 0.047                          | 0.001                      | 0.170                             |
| 4.875                         | 0.055                   | 0.049                          | 0.026                      | 0.182                             |
| 5.245                         | 0.074                   | 0.049                          | 0.115                      | 0.188                             |
| 5.615                         | 0.020                   | 0.048                          | -0.047                     | 0.176                             |
| 5.984                         | 0.012                   | 0.046                          | -0.236                     | 0.160                             |
| 6.354                         | 0.015                   | 0.045                          | -0.268                     | 0.155                             |
| 6.724                         | 0.035                   | 0.044                          | -0.233                     | 0.154                             |
| 7.094                         | -0.030                  | 0.041                          | -0.155                     | 0.142                             |
| 7.463                         | 0.027                   | 0.041                          | -0.161                     | 0.146                             |
| 7.833                         | 0.016                   | 0.039                          | -0.189                     | 0.138                             |
| 8.203                         | -0.052                  | 0.036                          | 0.036                      | 0.129                             |
| 8.572                         | 0.033                   | 0.035                          | -0.262                     | 0.122                             |
| 8.942                         | 0.006                   | 0.034                          | -0.184                     | 0.118                             |
| 9.312                         | -0.068                  | 0.031                          | -0.071                     | 0.107                             |
| 9.682                         | -0.066                  | 0.029                          | -0.011                     | 0.104                             |
| 10.051                        | -0.146                  | 0.026                          | 0.113                      | 0.094                             |
| 10.421                        | -0.156                  | 0.023                          | 0.172                      | 0.083                             |
| 10.791                        | -0.179                  | 0.019                          | 0.201                      | 0.070                             |
| 11.160                        | -0.113                  | 0.022                          | 0.175                      | 0.080                             |
| 11.530                        | -0.090                  | 0.045                          | 0.152                      | 0.163                             |

Table B.2:  $\theta_p^{\text{lab}} = 30^\circ$ 

| $E_p(\text{MeV})$ | $A_y$  | $\Delta A_y$ | $A_{yy}$ | $\Delta A_{yy}$ |
|-------------------|--------|--------------|----------|-----------------|
| 4.603             | 0.002  | 0.038        | 0.093    | 0.120           |
| 5.023             | 0.015  | 0.031        | -0.010   | 0.104           |
| 5.443             | 0.014  | 0.031        | 0.081    | 0.099           |
| 5.863             | 0.003  | 0.032        | -0.137   | 0.112           |
| 6.283             | -0.013 | 0.032        | -0.080   | 0.110           |
| 6.703             | -0.060 | 0.032        | -0.110   | 0.112           |
| 7.123             | -0.119 | 0.032        | -0.155   | 0.115           |
| 7.543             | -0.144 | 0.034        | -0.199   | 0.118           |
| 7.963             | -0.177 | 0.032        | -0.177   | 0.114           |
| 8.383             | -0.225 | 0.034        | -0.192   | 0.115           |
| 8.803             | -0.243 | 0.032        | -0.138   | 0.107           |
| 9.223             | -0.298 | 0.031        | -0.146   | 0.102           |
| 9.643             | -0.323 | 0.029        | -0.034   | 0.088           |
| 10.063            | -0.303 | 0.024        | 0.121    | 0.070           |
| 10.483            | -0.329 | 0.025        | 0.359    | 0.058           |
| 10.903            | -0.294 | 0.042        | 0.389    | 0.096           |

Table B.3:  $\theta_p^{\text{lab}} = 35^\circ$

| $E_p$ (MeV) | $A_y$  | $\Delta A_y$ | $A_{yy}$ | $\Delta A_{yy}$ |
|-------------|--------|--------------|----------|-----------------|
| 4.603       | 0.015  | 0.041        | 0.092    | 0.083           |
| 5.023       | -0.007 | 0.033        | 0.043    | 0.068           |
| 5.443       | 0.015  | 0.033        | 0.001    | 0.070           |
| 5.863       | -0.001 | 0.033        | 0.021    | 0.070           |
| 6.283       | -0.066 | 0.033        | -0.056   | 0.075           |
| 6.703       | -0.100 | 0.035        | -0.094   | 0.080           |
| 7.123       | -0.156 | 0.034        | -0.062   | 0.078           |
| 7.543       | -0.185 | 0.037        | -0.134   | 0.082           |
| 7.963       | -0.231 | 0.036        | -0.157   | 0.083           |
| 8.383       | -0.294 | 0.037        | -0.161   | 0.082           |
| 8.803       | -0.337 | 0.037        | -0.129   | 0.079           |
| 9.223       | -0.348 | 0.034        | -0.137   | 0.074           |
| 9.643       | -0.381 | 0.030        | -0.011   | 0.060           |
| 10.063      | -0.423 | 0.029        | 0.007    | 0.054           |
| 10.483      | -0.382 | 0.038        | 0.130    | 0.065           |
| 10.903      | -0.241 | 0.077        | -        | -               |

Table B.4:  $\theta_p^{\text{lab}} = 40^\circ$ 

| $E_p$ (MeV) | $A_y$  | $\Delta A_y$ | $A_{yy}$ | $\Delta A_{yy}$ |
|-------------|--------|--------------|----------|-----------------|
| 4.603       | -0.027 | 0.053        | 0.103    | 0.108           |
| 5.023       | -0.017 | 0.042        | 0.066    | 0.088           |
| 5.443       | -0.002 | 0.043        | 0.063    | 0.089           |
| 5.863       | -0.072 | 0.045        | 0.017    | 0.092           |
| 6.283       | -0.093 | 0.047        | -0.181   | 0.106           |
| 6.703       | -0.120 | 0.049        | -0.172   | 0.109           |
| 7.123       | -0.174 | 0.052        | -0.240   | 0.113           |
| 7.543       | -0.205 | 0.055        | -0.381   | 0.126           |
| 7.963       | -0.288 | 0.057        | -0.153   | 0.110           |
| 8.383       | -0.336 | 0.076        | -0.289   | 0.115           |
| 8.803       | -0.370 | 0.058        | -0.180   | 0.103           |
| 9.223       | -0.407 | 0.055        | -0.096   | 0.087           |
| 9.643       | -0.427 | 0.047        | -0.175   | 0.079           |
| 10.063      | -0.442 | 0.071        | -0.035   | 0.102           |

APPENDIX C

A POST-SUBMISSION NOTE IN CONNECTION

WITH CHAPTER ONE

In the time period between the submission of this thesis and the oral examination, Slaus et al. (1983) have reported a study of the  ${}^4\text{He}(\vec{d},\alpha p)n$  reaction at 12 and 17 MeV. This work has been drawn to the attention of this author by McKee (McKee, 1983). In view of the fact that this is closely related to the subject of chapter one of this thesis a few comments are necessary.

Slaus et al. (1983) in their kinematically complete experiment at 12 and 17 MeV report disagreement of their measurements with the predictions of the three-body model of Koike (1980) as far as the tensor analysing powers are concerned. The disagreement is particularly serious at 12 MeV incident deuteron energy. Some improvement results at 17 MeV but the  $A_{yy}$  measurements at  $\theta_{\alpha}^{\text{lab}} = 20^{\circ}$ ,  $\theta_p^{\text{lab}} = 120^{\circ}$  continue to be poorly represented by the three-body model. The authors conclude that tensor analysing powers are sensitive observables with which to study the input two-body interaction and the reaction mechanism. This, together with the findings of Ishikawa et al. (1982) give an independent support to the conclusions drawn in section (1.4) of this thesis.

REFERENCES

- T. Åberg, K.A. Jamison and P. Richard, Phys. Rev. Letts., 37, 63 (1976).
- M.S.A.L. Al-Ghazi, J. Birchall and J.S.C. McKee, Phys. Rev. A 25,  
3072 (1982).
- M.S.A.L. Al-Ghazi and J.S.C. McKee, Nucl. Instr. & Meth. 197, 117 (1982).
- M.S.A.L. Al-Ghazi, J.S.C. McKee and W.D. Ramsay, I.E.E.E. Trans. on  
Nucl. Sci. NS-26 #2, 2241 (1979).
- R.A. Arndt, D.D. Long and L.D. Roper, Nucl. Phys. A209, 429 (1973).
- R.A. Arndt and L.D. Roper, Nucl. Phys. A209, 447 (1973).
- S.L. Balasko and L.M. Brockman, University of Manitoba Cyclotron  
Laboratory Report p.92 (1981).
- H.A. Bethe and E.E. Salpeter, Handbuch der Physik (Springer, Berlin,  
1957), S. Flügge ed., Vol. 35, p.234.
- J. Birchall, J.J.G. Durocher, J.S.C. McKee, W.D. Ramsay and S.F.J. Wilk,  
J. Phys. G: Nucl. Phys. 4, 787 (1978).
- J. Birchall, N.T. Okumusoglu, M.S. de Jong, M.S.A.L. Al-Ghazi and  
J.S.C. McKee, Proceedings of the Fifth International Symposium  
on Polarization Phenomena in Nuclear Physics, Santa Fé,  
New Mexico (U.S.A.) 1980, Paper 5.32.
- J.P. Briand, Phys. Rev. Letts. 37, 656 (1976).

K.L. Brown, SLAC Report #75 (1972).

R.E. Brown, W. Grübler, R.A. Hardekopf, F.D. Corell, N. Jarmie and  
G.G. Ohlsen, Nucl. Phys. A331, 61 (1979).

H. Brückmann, W. Vogel, H.-W. Boie and U. Schröder, Proceedings of the  
Ninth International Conference on Cyclotrons and Their  
Applications (ed. G. Gendreau) p.719, (les éditions de physique,  
Cedex, France 1981).

E.J. Burge and D.A. Smith, Rev. Sci. Instr. 33, 137 (1962).

T.A. Cahill, Ann. Rev. Nucl. & Part. Sci 30, 211 (1980).

G. Cattapan, G. Pisent and V. Vanzani, Nucl. Phys. A241, 204 (1975).

B. Charnomordic, C. Fayard and G.H. Lamot, Phys. Rev. C 15, 861 (1977).

T.B. Clegg, Proceedings of the Symposium of Ion Sources and Formation of  
Ion Beams, Brookhaven National Laboratory, Upton (New York)  
BNL 50310, p.223 (1971).

J.A. Cookson, Nucl. Instr. & Meth. 165, 477 (1979).

J.A. Cookson and F.D. Pilling, Thin Solid Films 19, 381 (1973).

J.A. Cookson, A.T.G. Ferguson and F.D. Pilling, J. Radioanal. Chem.  
13, 39 (1972).

S.S. Dasgupta, R.J. Slobodrian, R. Roy, C. Rioux and F. Lahlou,  
Phys. Rev. C 22, 1815 (1980).

- G. Deconninck, G. Demortier and F. Bodart, "Atomic Energy Review",  
I.A.E.A. Vienna 1975, vol. 13, p.367.
- M.S. de Jong, Ph.D. Thesis, University of Manitoba (1981) (Unpublished).
- P. Doleschall, Nucl. Phys. A201, 264 (1973).
- A.D. Dymnikov, T. Ya Fishkova and S. Ya Yavor, Sov. Phys. - Tech. Phys.  
10, 340 (1965).
- L.D. Faddeev, Sov. Phys. J.E.T.P. 12, 1014 (1961).
- J.D. Garcia, R.J. Fortner and T.M. Kavanagh, Rev. Mod. Phys. 45, 111  
(1973).
- J.D. Garcia, E. Gerjuoy and J. Wekler, Phys. Rev. 165, 66 (1968).
- R.V. Gentry, T.A. Cahill, N.R. Fletcher, H.C. Kaufmann, L.R. Medsker,  
J.W. Nelson and F.G. Flocchini, Phys. Rev. Letts. 37, 11 (1976).
- A. Gervé and G. Schatz, Proceedings of the Seventh International  
Conference on Cyclotrons and Their Applications (ed. W. Joho)  
p.496, (Birkhäuser, Basel 1975).
- M. Gryzinski, Phys. Rev. 138 A336 (1965).
- J.M. Hansteen, O.M. Johnsen and L. Kocbach, At. Data and Nucl. Data  
Tables 15, 305 (1975).
- D. Heck, Karlsruhe Progress Report (1978).
- D. Heck, Karlsruhe Report KFK 2288 (April 1976).

W. Heisenberg, Z. Phys. 32, 841 (1925).

J.W. Humberston, R.L. Hall and T.A. Osborn, Phys. Letts. 27B, 195 (1968).

M. Ishikawa, S. Seki, K. Furuno, Y. Tagishi, M. Sawada, T. Sugiyama,  
K. Matsuda, J. Sanada and Y. Koike, J. Phys. Soc. Japan 51,  
1327 (1982).

Y. Isozumi, Phys. Rev. A 22, 1948 (1980).

T.B. Johansson, R. Akselsson and S.A.E. Johansson, Adv. X-ray Anal.  
15, 373 (1972).

T. Kambara, M. Takai, M. Takamura and S. Kobayashi, J. Phys. Soc.  
Japan 44, 704 (1978).

L.G. Keller and W. Haeberli, Nucl. Phys. A172, 625 (1971).

Q.C. Kessel and M.E. Rudd, Phys. Rev. A2, 1327 (1970).

H. Kneis, B. Martin, R. Nobile, B. Povh and K. Traxel, Nucl. Instr.  
& Meth. 197, 79 (1982).

H.D. Knox, R.G. Graves, F.N. Rad, M.L. Evans, L.C. Northcliffe,  
H. Nakamura and H. Noya, Phys. Letts. 56B, 33 (1975).

I. Koersner, L. Glantz, A. Johansson, B. Sundquist, H. Nakamura and  
H. Noya, Nucl. Phys. A286, 431 (1977).

Y. Koike, Y. Taniguchi, M. Sawada and J. Sanada, Prog. Theor. Phys.  
66, 1899 (1981).

Y. Koike, Nucl. Phys. A337, 23 (1980).

———, Prog. Theor. Phys. 59, 87 (1978a).

———, Nucl. Phys. A301, 411 (1978b).

J.M. Lambert, P.A. Treado, P.G. Roos, N.S. Chant, A. Nadasen, I. Slaus  
and Y. Koike, Phys. Rev. C 26, 357 (1982).

C. Lapointe, M.Sc. Thesis, University of Manitoba (1981) (Unpublished).

G.J.F. Legge, Nucl. Instr. & Meth. 197, 243 (1982).

D.E. Lobb, Nucl. Instr. & Meth. 86, 177 (1970).

Madison Convention, in Polarization Phenomena in Nuclear Reactions,  
H.H. Barschall and W. Haeberli (editors), University of  
Wisconsin Press, Madison (1971), p.XXV.

J.H. McGuire and P. Richard, Phys. Rev. A8, 1374 (1973).

J.S.C. McKee, Private Communication (1983).

J.S.C. McKee, C. Lapointe, J. Birchall, C. Pinsky and R. Bose,  
J. Environ. Sci. A16(5), 465 (1981).

J.S.C. McKee, Acta Physica Academiae Hungaricae, Tomus 33 (2), 167 (1973).

———, Rep. Prog. Phys. 33, 691 (1970).

H. Nakamura, H. Noya, S.E. Darden and S. Sen, Nucl. Phys. A305, 1 (1978).

R. Nobile, Y. Civelekoglu, B. Povh, D. Schwalm and K. Traxel, Nucl.  
Instr. & Meth. 130, 325 (1975).

- G.G. Ohlsen, Proceedings of the Fourth International Symposium on Polarization Phenomena in Nuclear Reactions, *Experientia Supplementum* 25, (Birkhäuser - Verlag, Zürich 1975) p. 287.
- G.G. Ohlsen and P.W. Keaton, Jr., *Nucl. Instr. & Meth.* 109, 41 (1973).
- G.G. Ohlsen, *Rep. Prog. Phys.* 35, 717 (1972).
- G.G. Ohlsen and P.G. Young, *Phys. Rev.* 136, B1632 (1964).
- H. Oswald, W. Burgmer, D. Gola, C. Heinrich, H.J. Helthen and H. Paetzgen. Schiek, *Phys. Rev. Letts.* 46, 307 (1981).
- C. Pinsky, University of Manitoba Cyclotron Laboratory Report p. 87 (1981).
- B.T. Price, C.C. Horten and K.T. Spinney, Radiation Shielding (Pergamon, Oxford 1957).
- W.D. Ramsay, M.S.A.L. Al-Ghazi, J. Birchall and J.S.C. McKee, *Phys. Letts.* 69A, 258 (1978).
- P.A. Schmelzbach, W. Grübler, V. König, R. Risler, D.O. Boerma and B. Jenny, *Nucl. Phys.* A264, 45 (1976).
- H. Shimizu, K. Imai, N. Tamura, K. Nisimura, K. Hatanaka, T. Saito, Y. Koike and Y. Taniguchi, *Nucl. Phys.* A382, 242 (1982).
- I. Slaus, J.M. Lambert, P.A. Treado, F.D. Correll, R.E. Brown, R.A. Hardekopf, N. Jarmie, Y. Koike and W. Grübler, *Nucl. Phys.* A397, 205 (1983).
- R.J. Slobodrian, *Rep. Prog. Phys.* 34, 175 (1971).
- C.A. Smith, "POLCA" A Program for the Calculation of Polarization Observables, User Library Program, Cyclotron Laboratory, University of Manitoba (1982).

Ch. Stoller, W. Wölfli, G. Bonani, M. Stöckli and M. Suter, Phys. Rev.  
A 15, 990 (1977).

Wm. J. Veigle, Atomic Data 5, 51 (1973).

J.P. Vinti, Phys. Rev. 42, 632 (1932).

R.E. Warner and R.W. Bercaw, Nucl. Phys. A172, 625 (1971).

S.F.J. Wilk, J.S.C. McKee and C.P. Randell, Nucl. Instr. & Meth. 142,  
33 (1977).

W. Wölfli and H.D. Betz, Phys. Rev. Letts. 37, 61 (1976).

W. Wölfli, Ch. Stoller, G. Bonani, M. Suter and M. Stöckli, Phys.  
Rev. Letts. 35, 656 (1975).

Y. Yamaguchi and Y. Yamaguchi, Phys. Rev. 95, 1635 (1954).